INVESTIGATION OF SOME PROPERTIES OF SPUTTERED ZnO THIN FILM

By

ABDULSALAM AJI SULEIMAN

THESIS PRESENTED TO

THE GRADUATE SCHOOL OF NATURAL AND APPLIED SCIENCE

OF

THE ABANT IZZET BAYSAL UNIVERSITY

IN PARTIAL FULFILLMENT OF THE REQUIREMENTS FOR THE DEGREE OF

MASTER OF SCIENCE

IN

THE DEPARTMENT OF PHYSICS

FEBRUARY, 2014

Approval of the Graduate School of Natural and Applied Science

Prof. Dr. Yaşar DÜRÜST

Director

I certify that this thesis satisfies the entire requirements as a thesis for the degree of Master of Science.

Prof. Dr. İbrahim BELENLİ

Head of Physics Department

This is to certify that we have read this thesis and in our opinion it is fully adequate, in scope and quality as a thesis and for the degree of Master of Science.

Prof. Dr. Ahmet VARİLCİ

Supervisor

Examining Committee Members

1. Prof. Dr. Ahmet VARİLCİ
2. Associate Prof. Dr. Osman GORUR
3. Assistant Prof. Dr. Gürcan YILDIRIM

ABSTRACT

INVESTIGATION OF SOME PROPERTIES OF SPUTTERED ZnO THIN FILM

Abdulsalam Aji SULEIMAN

Master of Science, Department of Physics

Supervisor: Prof. Dr. Ahmet VARİLCİ

February 2014, 51 Pages

The aim of this work was the study of sputtered zinc oxide (ZnO) film deposition, how the optical and structural properties of films based on the heated substrates during deposition can be altered. In recent years there has been increased interest in ZnO in terms of its potential applications. The electrical, optoelectronic and photochemical properties of ZnO thin film have resulted in its use for solar cells [8], transparent electrodes and blue/UV light emitting devices [9].

In this work, Zinc-Oxide (ZnO) thin films were deposited using reactive sputtering method. The reactive DC sputtering was performed with a Zinc (Zn) target and oxygen as a reactive gas, on an amorphous glass slides of few millimeters thickness. The effects of the increase in substrate temperature during deposition ranging from RT to 400 °C on the optical and structural properties of ZnO thin films have been studied. The crystalline structure, surface topology, and optical properties of the films were determined using X-ray diffraction (XRD), atomic force microscopy (AFM), and UV-Vis Spectrophotometer, respectively.

X-ray diffraction measure showed that the films with substrate temperatures from RT – 300^0C were single crystalline in nature with (002) *c-axis* oriented

crystallite of hexagonal wurtzite structure. However, as the temperature reached 400 °C the film appears to be polycrystalline with (100), (002), (101), (110) and (103) oriented crystallites of same hexagonal wurtzite structure. Crystalline property and grain size of the films were found to increase as the temperature of the substrate increases. The optical bandgap of the ZnO film were found red shifted in the range of 3.353 – 3.001 eV, as the substrates temperature increased bandgap energy of the films decreased. And according to the images taken by AFM, its shows that root mean square (rms) values of surface roughness for the films were in variation which shows a better smoothness as the temperature increases. And from the UV-Vis spectrophotometer, almost all the film showed transmittance over 80% in the visible light range spectrum, the transmittance decreases with the increase in the temperature. All the results indicate that, as the substrate temperature increases the films photoactive performance found to be increasing decreases with improve in roughness and smoothness on their surface.

Keywords: Semiconductors, thin film, ZnO, Band gap

ÖZET

ZnO INCE FİLMİN BAZI ÖZELLİKLERİNİN ARAŞTIRMASI

Abdulsalam Aji SULEIMAN

Yüksek Lisans, Fizik Bölümü

Tez Danişmanı: Prof. Dr. Ahmet VARİLCİ

Şubat 2015, 51 Sayfa

Bu tezdeki amacımız film oluşturma anında (insitu) altlık sıcaklığını değiştirerek ZnO ince filmin yapısal ve optik özelliklerini çalışmaktır. Son yılllarda ZnO üzerinde potansiyel uygulamalar arttığından, ZnO'ya ilgi, doğal olarak, artmıştır. ZnO ince filmin elektriksel, optoelektronik ve fotokimyasal özelliklerindeki gelişme onun güneş hücrelerinde[8], ışık geçirgen elektrotlarda ve mavi/UV ışık yayan diyotlarda [9] kullanımının önünü açmıştır.

Bu çalışmada, ZnO ince film DC magnetron saçtırma tekniği kullanılarak üretilmiştir. DC saçtırma yöntemi Zn hedef malzeme ve oksijen gazı kullanılarak amorf ve 1-2 mm kalınlığındaki cam üzerinde gerçekleştirildi. Film üretim esnasında altlık sıcaklığı oda sıcaklığından 400°C'a kadar değiştirilerek filmin optik ve yapısal özelliklerinin değişimi incelendi. Üretilen filmlerin kristal yapısı, yüzey morfolojisi ve optik özellikleri X Işını Kırınımmetresi (XRD), Atomik Kuvvet Mikroskobu (AFM) ve UV-Vis Spektrometresi kullanılarak incelendi.

XRD ölçümü altlık sıcaklığı oda sıcaklığından 300°C'a kadar olan filmlerin hegzagonal wurtzite yapısında ve (002) c ekseni yönlenmesine sahip olduğunu gösterdi. Ancak, film altlık sıcaklığı 400°C'a ulaştığında film polikristal hale dönüşüp aynı hegzagonal wurtzite yapısında (100), (002), (101), (110) ve (103)

yansımalarını gösterdiği görüldü. Üretilen bu filmlerin tane büyüklükleri ve Kristal özellikleri altlık sıcaklığı artışı ile arttığı gözlendi. ZnO filmin optic bant aralığı, altlık sıcaklığı arttarken 3.353 – 3.001 eV arasında azalarak değiştiği bulundu. AFM sonuçları, altlık sıcaklığı artarken filmin yüzey pürüzlüğünün rms değerlerinin daha düzgün bir prüzsüz yüzeye doğru gittiğini gösterdi. UV-Vis spektrometre sonuçları filmin görünür ışık bölgesinde %80 geçirgenlik gösterdiği ve altkık sıcaklığı yükseldikçe geçirgenliğin arttığı bulundu. Sonuç olarak altlık sıcaklığı arttıkça film kalitesi artmakta ve yüzey de önemli ölçüde iyileşmektedir**.**

Anahtar Kelimeler: Yarıiletken, ince film, ZnO, Bant aralığı

This thesis is dedicated to the memory of my father….

ACKNOWLEDGEMENT

With deep sense of gratitude, I wish to express my sincere thanks to my supervisor Prof. Dr. Ahmet VARİLCİ of The Department of Physics Abant İzzet Baysal University, for his excellent guidance and support throughout the work. I received very useful and excellent academic training from him, which has stood in good stead while writing this thesis. His unique inimitable style has left an indelible impression on me. His constant encouragement, help and review of the entire work during the course of the investigation are invaluable. Nevertheless, it helped me acquire and develop some of the skills and intricacies of good independent research.

I must express my deep appreciation and gratitude to Assistant Prof. Dr. Gürcan YILDIRIM of Mechanical engineering department for his constant and selfless support at every stage of my project work. Without his support and contributions, this project would have been difficult to complete.

My sincere thanks to all the faculty members, research members and friends for their encouragement and kind help extended toward me.

And finally I would like to share is moment of happiness with my family members for whom I do what I do.

TABLE OF CONTENTS

LIST OF FIGURES

Figures

Pages

LIST OF TABLES

Tables

ACRONYMS ANACRONYMS AND ABBREVIATION

A : Absorbance

AFM : Atomic force microscope

AC : Alternative current

CVD : Chemical Vapor Deposition

CB : Conduction Band

FCC : Face-centered-cubic lattice

DC : Direct current

d33 : Principal performance-determining parameter for piezoelectric Materials. Indicates charge per unit force in the polarization direction of the sample; the electric field and the strain are both along the Polarization axis.

EBE : Electron beam evaporation

EBL : Electron beam lithography

FWHM : Full width at half maximum

IC : Integrated circuits

JCPDS : Joint Committee on Powder Diffraction Standards

MBE : Molecular Beam Epitaxy

MOCVD: Metal-organic Chemical Vapor Deposition

NaCl : Sodium chloride

rms : root mean square

RF : Radio Frequency

RT : Room Temperature

SAW : Surface Acoustic Wave

SEM : Scanning Electron Microscopy

T : Transmission

TCO : Transparent Conductive Oxide

XRD : X-ray Diffraction

UV : Ultra Violet

VB : Valence Band

VIS : Visible

ZnO : Zinc Oxide

ZnS : Zinc sulfide

CHAPTER 1

INTRODUCTION

1.1 Introduction

A semiconductor can be considered a material having a conductivity ranging between an insulator and a metal. One of the crucial property of semiconductors is the bandgap; a range of forbidden energies within the electronic structure of the material. Semiconductors typically have band gaps ranging approximately between 1 and 4 eV, while insulators have larger band gaps, often greater than 5 eV [1]. The thermal energy available at room temperature, 24°C, is approximately 25 meV and is thus considerably smaller than the energy required to promote an electron across the band gap [2]. This means that there are a small number of carriers present at room temperature, due to the high energy tail of the Boltzmann-like thermal energy distribution [3]. It is the ability to control the number of charge carriers that makes semiconductors of great technological importance. Few of the best examples of semiconductors are Germanium and Silicon; they both have similar proprieties such as belonging to the same group of the periodic table and being both indirect band gap semiconductors, but silicon is more stable and preferable than germanium because, the valence electrons in germanium are in the fourth shell while those in silicon are in the third shell, closer to the nucleus. This means that the germanium valence electrons are at higher energy levels than those in silicon and, therefore, require a smaller amount of additional energy to escape from the atom. This property makes germanium more unstable at high temperature, and this is basic reason why silicon is the most widely used semi conductive material [4].

In the last 60 years or so, we have been shaped by the silicon age. The semiconductor industry is still a main driver of today's innovations. A life without semiconductors is unimaginable today: no information highway, no cell phones, no airbags in cars and no personal computers, etc. Besides silicon, which has been the semiconductor for the last 60 years, scientists have turned their efforts towards other

materials to fulfill the needs of various niche applications. It is a little known fact that the semiconducting properties of Zinc Oxide (ZnO) were already discovered in the 1920's. Then, ZnO crystals were used as diodes to rectify AM radio signals. Varistors (voltage dependent resistors) are commonly made by sintering of ZnO powder with added trace materials. This method was first reported in the 1950's [4, 5].

In recent years there has been increased interest in ZnO in terms of potential applications as piezoelectric films (or coatings) for surface acoustic wave devices (SAW) [6] , for IR and visible light emitting devices and UV sensing [7], which was reported in 1986 . The electrical, optoelectronic and photochemical properties of undoped ZnO have resulted in its use for solar cells [8], transparent electrodes and blue/UV light emitting devices [9]. ZnO is a unique material that exhibits both semiconducting and piezoelectric properties. In the past decade, numerous studies have been made on both production and application of one-dimensional ZnO. ZnO nanomaterial is promising candidates for Nano electronic and photonics. Compared with other semiconductor materials, ZnO has a high exciton binding energy of 60 meV [10], which gives it a high potential for room temperature light emission. It is more resistant to radiation and is multifunctional as it has piezoelectric, ferroelectric and ferromagnetic properties [11]. ZnO-based semiconductor and nanowire devices are also promising for integration on a single chip. So far, the various applications of ZnO nanomaterials such as biosensors [12], UV detectors [13] and field emission displays are being developed.

ZnO can be deposited on a substrate using various methods, such as sputtering, pulsed laser deposition (PLD), molecular beam epitaxy (MBE), chemical vapor deposition (CVD), metal organic CVD (MOCVD) and sol-gel. During these studies, we have been producing ZnO films using sputtering, as this technique offers relatively fast deposition rates.

1.2 Crystal Structure

Most of the group II-VI binary compound semiconductors crystallize in either cubic zinc-blende or hexagonal wurtzite structure where each anion is surrounded by

four cations at the corners of a tetrahedron, and vice versa. This tetrahedral coordination is typical of sp^3 covalent bonding, but these materials also have a substantial ionic character. ZnO is an II-VI compound semiconductor whose ionicity resides at the borderline between covalent and ionic semiconductor. The crystal structures shared by ZnO are wurtzite B4, zinc blende B3, and rock salt B1, as schematically shown in Fig. 1. At ambient conditions, the thermodynamically stable phase is wurtzite. The zinc-blende ZnO structure can be stabilized only by growth on cubic substrates, and the rock salt NaCl structure may be obtained at relatively high pressures.

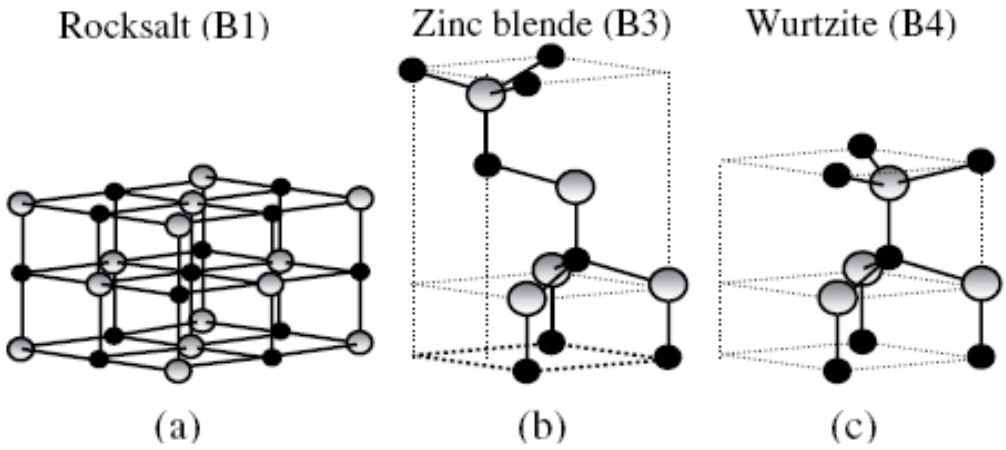

Figure 1: Stick and ball representation of ZnO crystal structures: (a) cubic rock salt (B1), (b) cubic zinc blende (B3), and (c) hexagonal wurtzite (B4). Shaded gray and black spheres denote Zn and O atoms, respectively.

Zinc oxide hexagonal wurtzite-type structure has a polar hexagonal axis, the *c-axis*, chosen to be parallel to *z*. The primitive translation vectors *a* and *b* lay in the *x–y* plane, are of equal length, and include an angle of 120°, while *c* is parallel to the *z-axis*. The point group is in the various notations 6mm or C_{6v}, the space group $P6_3mc$ or C^4_{6v}. One zinc ion is surrounded tetrahedral by four oxygen ions and vice versa. The primitive unit cell contains two formula units of ZnO. The values of the primitive translation vectors are at room temperature $a = b \approx 0.3249$ nm and $c \approx 0.5206$ nm. The ratio *c/a* of the elementary translation vectors deviates with values around 1.602 slightly from the ideal value $c/a = 8/3 = 1.633$. In contrast to other II–VI semiconductors, which exist both in the cubic zinc blende and the hexagonal wurtzite-type structures (like ZnS, which gave the name to both structures) ZnO

crystallizes with great preference in the wurtzite-type structure. The two latter structures both form a face-centered cubic lattice (FCC), however with different arrangements of the atoms within the unit cell, i.e. different bases.

1.3 Lattice Parameters

The lattice parameters of a semiconductor usually depend on the following factors:

- Free electron concentration acting via deformation potential of a conduction band minimum occupied by these electrons.
- Concentration of foreign atoms and defects and their difference of ionic radii with respect to the substituted matrix ion.
- External strains (for example, those induced by substrate).
- Temperature.

The lattice parameters of any crystalline material are commonly and most accurately measured by high resolution x-ray diffraction (HRXRD) by using the Bond method [14] for a set of symmetrical and asymmetrical reflections.

For the wurtzite ZnO, lattice constants at room temperature determined by various experimental measurements and theoretical calculations are in good agreement. The lattice constants mostly range from 3.2475 to 3.2501 Å for the *a* parameter and from 5.2042 to 5.2075 Å for the *c* parameter. The *c/a* ratio vary in a slightly wider range, from 1.593 to 1.6035 .The deviation from that of the ideal wurtzite crystal is probably due to lattice stability and ionicity. It has been reported that free charge is the dominant factor responsible for expanding the lattice proportional to the deformation potential of the conduction-band minimum and inversely proportional to the carrier density and bulk modulus. The point defects such as zinc antisites, oxygen vacancies, and extended defects, such as threading dislocations, also increase the lattice constant.

For the zinc-blende 4olytypes of ZnO, the calculated lattice constants based on a modern *ab initio* technique are predicted to be 4.60 and 4.619 Å. Ashrafi et al. [15]

characterized the zinc-blende phase of ZnO films grown by plasma assisted metal organic molecular beam epitaxy using reflection high-energy electron-diffraction (RHEED), x-ray diffraction (XRD), transmission electron microscope (TEM), and atomic-force microscope (AFM) measurements.

A high-pressure phase transition from the wurtzite to the rocksalt structure decreases the lattice constant down to the range of 4.27 – 4.294 Å. The experimental values obtained by x-ray diffraction are in close agreement. The predicted lattice parameters of 4.058–4.316 Å using various calculation techniques, such as the HF, are about 5% smaller or larger than the experimental values.

Table 1: Properties of Zinc Oxide (ZnO)

Physical Parameters	**Values**
Crystal structure	Hexagonal, wurtzite
Molecular weight	Zn:65.38, O:16 and ZnO:81.38
Lattice constant	a = 3.246 Å, c = 5.207 Å
Density	5.67 g/cm^3
Cohesive energy	E_{coh} = 1.89eV
Melting point	Tm = 2250 ^{0}K under pressure
Heat fusion	4,470 cal/mole
Thermal conductivity	25 W/mK at 20 ^{0}C
Thermal expansion coefficient	4.3 x 10^{-6} / ^{0}K at 20 ^{0}C
Band gap energy at RT	3.37 eV
Reflective Index	2.008
Debye temperature	370 ^{0}K
Electron and Hole effective mass	m_e* = 0.28, m_h* = 0.59
Lattice energy	964 kcal/mole
Dielectric constant	ε_0 = 8.75, ε_∞ = 3.75
Exciton Binding energy	E_b = 60 meV
Pyroelectric constant	6.8 Amp./sec./cm^2/^{0}K x 10^{10}
Piezoelectric coefficient	D_{33} = 12 pC/N

1.4 Electronic band Structure

The band structure of a given semiconductor is pivotal in determining its potential utility. Consequently, an accurate knowledge of the band structure is critical if the semiconductor in question is to be incorporated in the family of materials considered for device application. Several theoretical approaches of varying degrees of complexity have been employed to calculate the band structure of ZnO for its

wurzite, zinc-blende, and rocksalt polytypes. Besides, a number of experimental data have been published regarding the band structure of the electronic band structure of the electronic states of wurtzite ZnO. X-ray or UV reflection/absorption or emission techniques have conventionally been used to measure the electronic core levels in solids. These methods basically measure the energy difference by inducing transitions between electronic levels (for example, transitions from the upper valence-band states to the upper conduction-band states, and from the lower valence-band states) or by exciting collective modes (for example, the upper core states to the lower edge of the conduction band and to excitations of plasmons). Another important method for the investigation of the energy region is based on the photoelectric effect extended to the x-ray region, namely, photoelectron spectroscopy (PES). The peaks in emission spectrum correspond to electron emission from a core level without inelastic scattering, which is usually accompanied by a far-less-intense tail region in the spectrum. More recently, angle-resolved photoelectron spectroscopy (ARPES) technique has started to be used. This technique together with synchrotron radiation excitation has been recognized as a powerful tool that enables experimental bulk and surface electronic band structure determinations under the assumptions of k conservation and single nearly-free-electron-like final band.

Since ZnO is a direct gap semiconductor with the global extrema of the uppermost valence and the lowest conduction bands (VB and CB, respectively) at the same point in the Brillouin zone, namely at $k = 0$, i.e. at the Γ-point, we are mainly interested in this region. The lowest CB is formed from the empty 4s states of Zn^{2+}or the anti-bonding sp^3 hybrid states. A typical representation of the band structure looks as follows [16]:

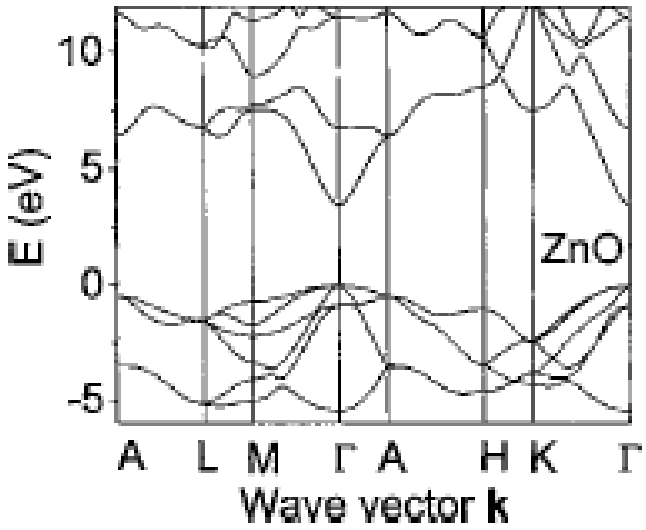

Figure 2: Band diagram of ZnO

1.5 Piezoelectricity and Ferro electricity

All materials undergo a change in dimension when they are exposed to an electric field. This phenomenon is called electrostriction; the induced strain is proportional to the square of the electric field. While generally considered to be an exclusive property of crystalline dielectrics, the phenomenon is also observed in amorphous solids and liquids. However, the reverse effect does not occur in all materials, i.e. most do not develop an electric polarization when they are strained by an external stress. The materials that do not exhibit the reverse effect belong to the 11 crystal classes that possess a center of symmetry. The materials belonging to the remaining 21 point groups have a non-Centro-symmetric structure and exhibit the reverse effect, except the materials from the cubic class (432) which possesses symmetry characteristics which combine to give no reverse effect. The materials that show the reverse effect are piezoelectric. To a first approximation the polarization is proportional to the stress and the effect is direct. Piezoelectric materials also show the so-called converse effect, as the development of a strain is proportional to the applied field. The converse effect is superimposed to the electrostrictive effect. Among the 20 piezoelectric crystal classes, a subdivision can be made between the 10 classes which contain a unique polar axis in the unstrained conditions and the 10

classes that have no such polar axis. Quartz is an example of a piezoelectric material without a polar axis in the unstrained state. In that case the dipolar arrangement occurs in several compensating directions so that there is no net crystal dipole. When stress is applied, the symmetry is disturbed and a direction is favored, giving rise to a net polarization and to the piezoelectric effect. The piezoelectric materials which possess a polar axis in the unstrained conditions are called pyro electric. When pyro electric materials are heated, they expand and the magnitude of the net dipole changes with the temperature, so that compensating charges appear on the two opposite faces of the crystal. ZnO is a pyro electric material. Pyro electric materials can be subdivided again in two classes. The ferroelectric materials are defined as those pyro electric materials for which the polar axis can be realigned in another direction by an external electric field.

ZnO clearly has piezoelectric properties and is subject to electrostriction. It appears that electrostriction in ZnO has not been investigated in detail as a literature search showed no related publications.

CHAPTER 2

THIN FILM GROWTH TECHNIQUES

2.1 Introduction

The vast varieties of thin film materials, their deposition processing and fabrication techniques, spectroscopic characterization, and optical characterization, probes that are used to produce the devices. It is possible to classify these techniques in two ways [17, 18].

- Physical Process
- Chemical Process.

Physical method covers the deposition techniques which depend on the evaporation or ejection of the material from a source, i.e. evaporation or sputtering, whereas chemical methods depend on physical properties. Structure-property relationships are the key features of such devices and basis of thin film technologies. Underlying the performance and economics of thin film components are the manufacturing techniques on a specific chemical reaction [19]. Thus chemical reactions may depend on thermal effects, as in vapor phase deposition and thermal growth. However, in all these cases a definite chemical reaction is required to obtain the final film.

When one seeks to classify deposition of films by chemical methods, one finds that they can be classified into two classes. The first of these classes is concerned with the chemical formation of the film from medium, and typical methods involved are electroplating, chemical reduction plating and vapor phase deposition. A second class is that of formation of this film from the precursor ingredients e.g. iodization, gaseous iodization, thermal growth, sputtering ion beam implantation, CVD, MOCVD and vacuum evaporation.

The methods summarized in table 2.1 are often capable of producing films defined as thin films, i.e. 1 µm or less and films defined as thick films, i.e. 1 µm or more. However, there are certain techniques which are only capable of producing thick films and these include screen printing, glazing, electrophoretic deposition, flame spraying and painting.

Table 2: Classification of Thin Film Deposition Techniques

Thin Film Deposition Techniques

Physical | Chemical

Sputtering	Evaporation	Gas Phase	Liquid Phase
Glow Discharge DC Sputtering	Vacuum Evaporation	Chemical Vapor Deposition	Electro-deposition
Triode Sputtering	Resistive heating Evaporation	Laser Chemical Vapor deposition	Chemical Bath Deposition (CBD)
Getter Sputtering	Flash Evaporation	Photo-chemical Vapor deposition	Electro less Deposition
Radio frequency Sputtering	Electron beam Evaporation	Plasma enhanced Vapor deposition	Anodisation
			Liquid phase Epitaxy
Magnetron Sputtering	Laser Evaporation	Metal-organic Chemical vapor Deposition (MOCVD)	Sol-gel
			Spin coating
Ion Beam Sputtering			Spray-pyrolysis Technique (SPT)
A.C Sputtering	Arc		Ultrasonic SPT
	R.F Heating		Polymer assisted Deposition (PAD)

2.2 Physical Processes

2.2.1 Sputtering

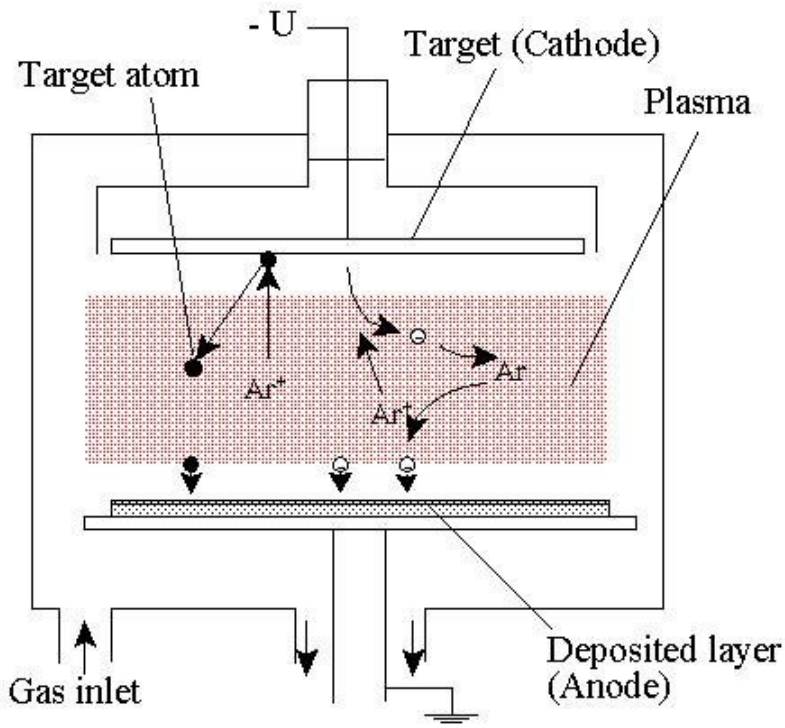

Figure 3: Schematic diagram of sputtering chamber.

As shown in figure 2 the sputter target of the material to be sputtered is the cathode of the system and the substrate/substrate holder is the anode, which is in the lower part of the chamber.

Once the vacuum chamber is evacuated to the desired level, a sputtering gas (usually Argon) is introduce. The background pressure is nomally in Torr range. The reactive sputtering is achieved by adding O_2 to form oxides, H_2 to form hydrogenated material, or N_2 to form nitrides. The stoichiometry of the sputtered film can be set by varying the ratio of the introduced gases. A large negative potential between target and ground initiates the process and electrons will be emitted from the target surface. Typical voltage ranges from 100 Volts to 1 kV. The ejected electrons are accelerated through the potential and get a very high kinetic energy. They collide with the gas molecules and ionise them. The positive ions are accelerated towards the cathode. On

hitting the target surface, part of the energy is transformed into heat and part is transferred to other particles. These particles can eventually get enough energy to leave the target surface. Various particles are eventually emitted: neutral atoms which will eventually reach the substrate and build the film, negative ions, photons and secondary electrons. The secondary electrons will again be accelerated from the target and ionise more gas atoms that will sputter the target and so on. The secondary electron yield needs to be high enough in order to maintain the plasma. When the substrate is immersed into the plasma (shutter removed), the electrons cover the surface much faster than the ions. A negative potential develops which attracts the ions and repels the electrons. Around the substrate an electron depleted sheet forms up to a steady state when the ionic current equals to the electron current. The target has always the strongest negative potential.

The bombardment is a key parameter in the sputtering deposition. It has at least three major effects. Firstly, it heats the substrate. The temperature of a substrate immersed in plasma will rise up to 150 ºC [23, 24]. This thermal energy enhances the surface mobility of the atoms and has an influence on the growth of the film. Secondly, the energy of a bombarding particle can be directly transferred to an atom of the surface through momentum transfer in a collision. It will also increase its mobility, which can lead to resputtering of the atom from the surface [20]. Thirdly, if the energy of the bombarding particle is too high, it can damage the film by the creation of defects during its implantation in the film. The bombardment is also influenced by the nature and pressure of the sputtering gas, the sputtering distance and the sputtering angle.

Futhermore, this happen to be one of the most fastest way of depositing a thin films among the other techniques. And is the method we used throughout this study.

2.2.2 Pulsed Laser Deposition (PLD)

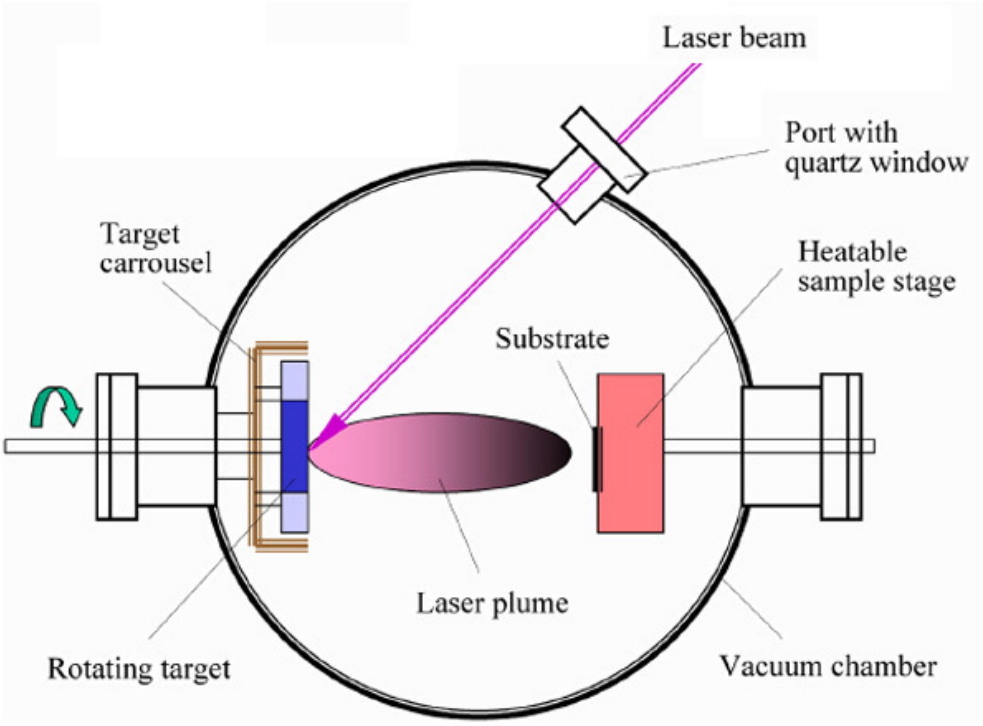

Figure 4: Schematic representation of PLD.

Pulsed Laser Deposition (PLD) is a thin film deposition technique where a pulsed laser beam is focused onto a pellet of material of which a thin film is desired. This pellet of source material, called the target, is heated locally by the high energy density of the laser light. The energy density on the target surface causes extreme heating of a small volume. The amount of heating depends on the absorption depth of the light, which is a function of the laser wavelength and the used target material. This local heating, results in the creation of a plasma without any melt phase which is called ablation. The amount of heat transported into the target is minimized due to the instantaneous character of the pulsed laser. The thermal diffusion length is defined as [21,22]:

$$l_{th}$$

with κ being the thermal diffusion coefficient, ρ the density of the target, c_p the specific heat and τ_l the convection time. This time for convection is often shorter

than the laser pulse, resulting in hardly any heating of the target. This holds particularly for oxides which often have a low thermal diffusion coefficient.

The evaporation process takes place in ~1 nanosecond. During this evaporation time a small volume of target material with a depth of the laser wavelength is evaporated. Typically this is only a fraction of the pulse duration of the lasers often used in PLD. This small evaporated volume is then heated by the remainder of the laser pulse resulting in a plasma of high temperature and pressure. During the evaporation and heating process, hardly any expansion takes place. Expansion is driven by the high pressure in this small volume of the initial plasma. The evaporated material is collected on the substrate material opposite to the target where a thin film is formed. This substrate material is mounted onto a heater for the depositions of thin films at elevated temperatures.

2.3 Chemical Processes

2.3.1 Molecular Beam Epitaxy (MBE)

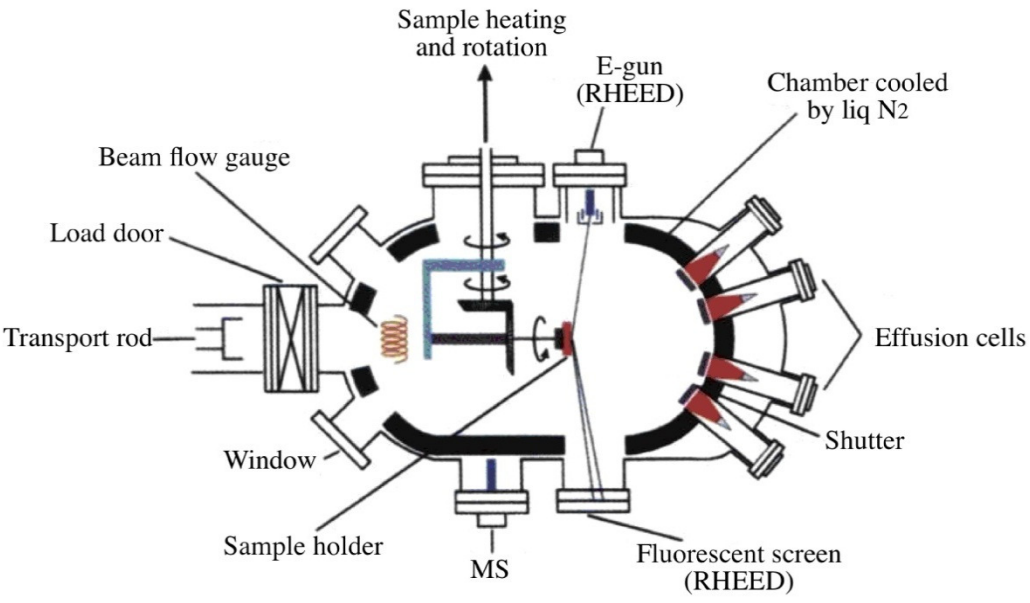

Figure 5: Schematic diagram of MBE.

Molecular beam epitaxy is a technique for epitaxial growth via the interaction of one or several molecular or atomic beams that occurs on a surface of a heated crystalline substrate. In Fig. 4 a scheme of a typical MBE system is shown. The solid

sources materials are placed in evaporation cells to provide an angular distribution of atoms or molecules in a beam. The substrate is heated to the necessary temperature and, when needed, continuously rotated to improve the growth homogeneity [23, 24]. The molecular beams are typically from thermally evaporated elemental sources. For example, in solid-source MBE, elements such as gallium and arsenic, in there pure form, are heated in separate quasi-Knudsen effusion cells until they begin to slowly sublime. The gaseous elements then condense on a substrate where they may react with each other, which result a single-crystal gallium arsenide thin film [24].

2.3.2 Chemical Vapour Deposition (CVD)

A reaction chamber is used for this process too, into which the reactant gases are introduced to decompose and react with the substrate to form the film [25]. Is the predefined mix of reactant gases and diluent inert gases introduced at a specified flow rate into the reaction chamber, the gas species move to the substrate and the reactants get adsorbed on the surface of the substrate, the reactants undergo chemical reactions with the substrate to form the film then the gaseous by-products of the reactions are desorbed and evacuated from the reaction chamber [26]

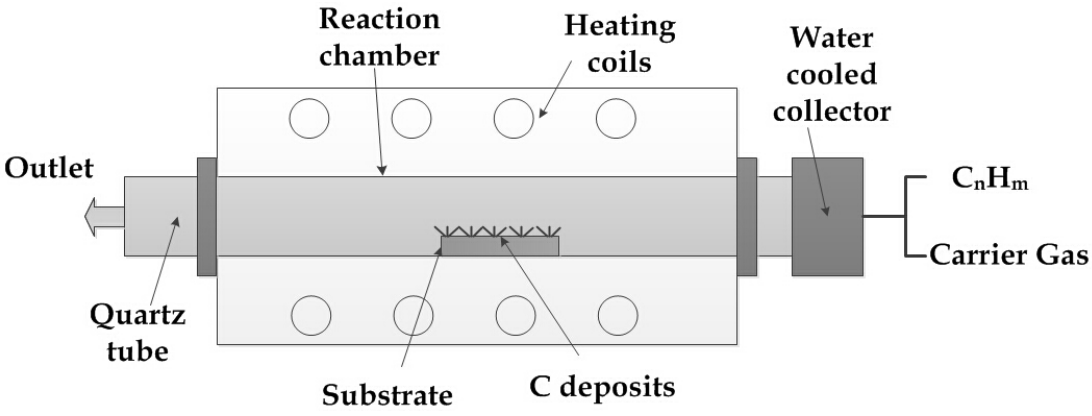

Figure 6: Simple illustration of Chemical Vapor Deposition (CVD) technique.

CHAPTER 3

CHARACTERIZATION TECHNIQUES

3.1 Introduction

Characterization is an important step in the development of exotic materials. The complete characterization of any material consists of phase analysis, compositional characterization, structural elucidation, micro-structural analysis and surface characterization, which have strong bearing on the properties of materials. This has led to the emergence of variety of advanced techniques in the field of materials science. In this section different analytical instrumental techniques used to characterize our thin films are described with relevant principles of their operation and working.

3.2 X-ray Diffraction

X-ray diffraction (XRD) is a versatile, non-destructive analytical technique for identification and quantitative determination of the various crystalline compounds, known as 'phases', present in solid materials and powders. Diffraction is due essentially to the existence of certain phase relations. It is well known that two rays are completely in phase whenever their path lengths differ by either zero of a whole number of wavelengths. Differences in the path length of various rays arise quite naturally considering how a crystal diffracts X-rays. Figure 14 shows the diffraction of a beam of parallel and monochromatic X-rays of wavelength λ is incident on a crystal at an angle θ, also known as Bragg angle, which is measured between the direction of the incident beam and the crystal plane under consideration.

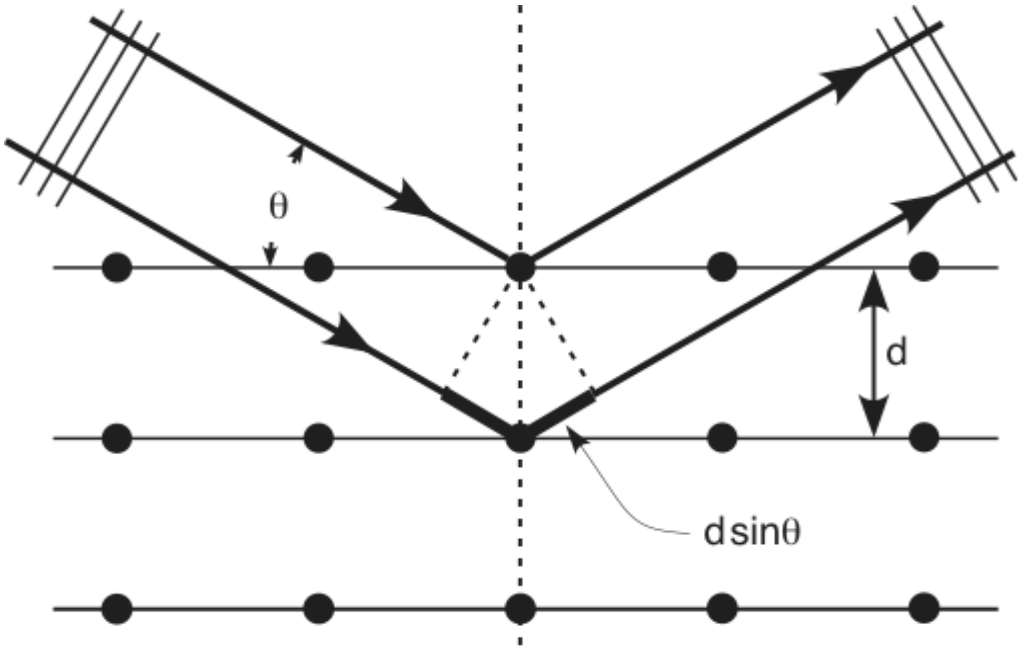

Figure 7: Diffraction of X-rays by a crystal.

The interaction with the first of these planes produces a reflected component at the specular reflection angle θ, which is rather weak if the X-rays are deeply penetrating. For the second and all subsequent planes, there are similar components of reflected energy at the specular angle θ. It can be seen from Figure 14 that the additional path of the lower ray compared to the upper ray is 2d sin θ. Consequently all reflected components can interfere constructively in phase if this distance is a multiple of the wavelength. This condition for efficient specular reflection is known as Bragg's law

$$2d \sin\theta = \lambda n,$$

Where n is an integer. Since the atomic arrangement is identical in all the planes under consideration, the Bragg diffraction condition depends on the spacing of the planes but is independent of the atomic arrangement within each plane. Since sin θ cannot exceed unity, the basic condition n $\lambda < 2d$ must be satisfied to obtain any diffraction. For a spacing between planes in the order of 3 Å, cannot exceed 6 Å. On the other hand if is much smaller than d, the diffraction angles are too small to be conveniently measured. Experimentally, by using X-rays of known wavelength and

measuring the spacing d of the planes in a crystal can be determined through Bragg's law [27].

For thin films, the powder technique in conjunction with diffractometer is most commonly used. In this technique the diffracted radiation is detected by the counter tube, which moves along the angular range of reflections. The intensities are recorded on a computer system. The'd' values are calculated using relation (2.8) for θ known values of λ, and n. The X- ray diffraction data thus obtained is printed in tabular form on paper and is compared with Joint Committee Power Diffraction Standards (JCPDS) data to identify the unknown material. The sample used may be powder, single crystal or thin film. The crystallite size of the deposits is estimated from the full width at half maximum (FWHM) of the most intense diffraction line by Scherrer's formula as follows [28]

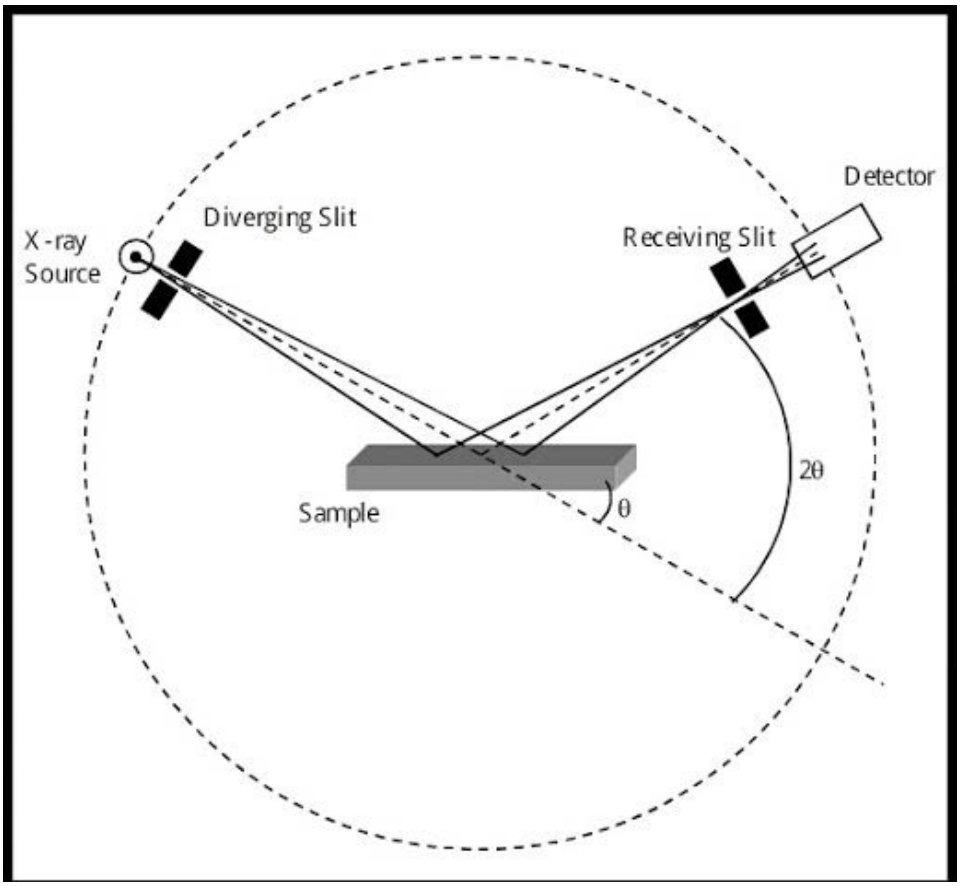

Figure 8: Schematics of X-ray diffractometer.

3.3 Atomic Force Microscopy imaging

The atomic force microscopy (AFM) probes the surface of a sample with a sharp tip, a couple of microns long often less than 100 Å in diameter. The tip is located at the free end of a cantilever, which is 100 to 200 μm long. The forces between the tip and sample surface cause the cantilever to bend or deflect. A detector measures the cantilever deflection as tip is scanned over the sample or the sample is scanned under the tip. The measured cantilever deflection allows a computer to generate a map or surface topography.

Several forces typically contribute to the deflection of an AFM cantilever. AFM operates by measuring the attractive or repulsive forces between a tip and the sample. The forces most commonly associated with atomic force microscopy are interatomic force called the Van der Waals force. The dependence of the Van der Waals force upon the distance between the tip and the sample is shown in figure 16. The two distance regimes are labeled in the figure are (a) the contact regime and (b) non-contact regime. In the contact regime, the cantilever is held at a distance less than few angstroms from the sample surface, and the inter-atomic force between the cantilever and the sample is repulsive. In the non-contact regime, the cantilever is held at a distance of the order of tens to hundreds of angstroms from the sample surface, and the inter-atomic force between the cantilever and sample is attractive. Figure 17 shows schematic diagram of AFM [29, 30].

In principle, AFM resembles the record player as well as the surface profilometer. However, AFM incorporates a number of refinements that enable it to achieve atomic–scale resolution: Sensitive detection, flexible cantilever, sharp tips, high-resolution tip sample positioning and Force feedback

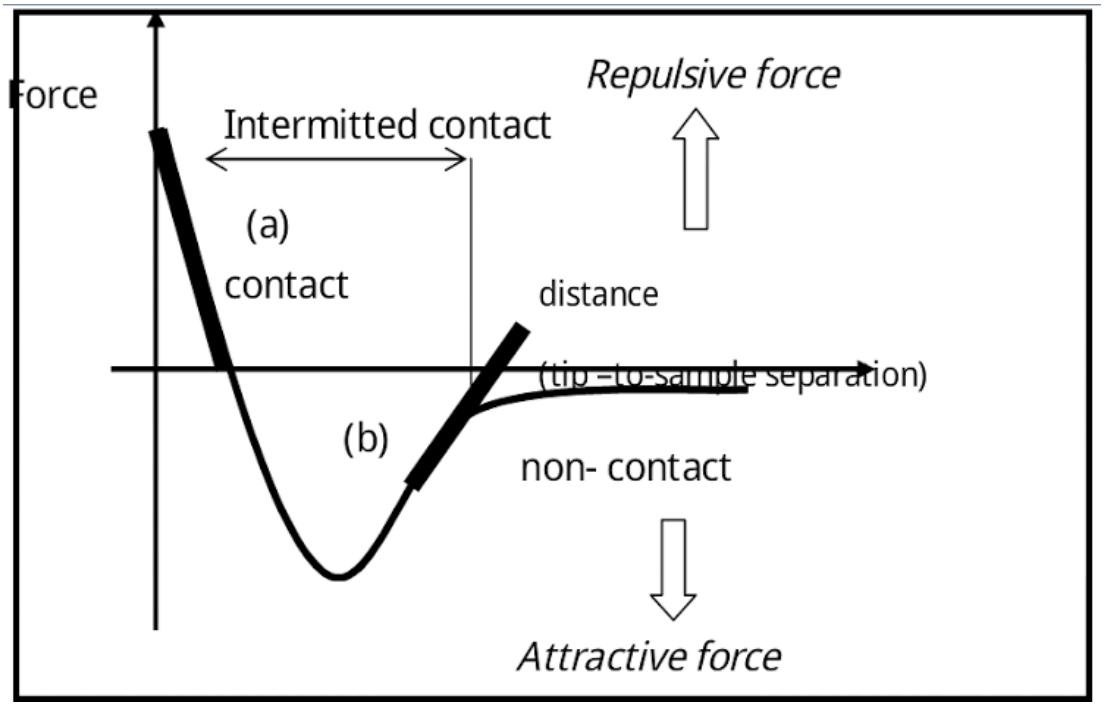

Figure 9: Inter-atomic forces versus distance curve for the operation of AFM

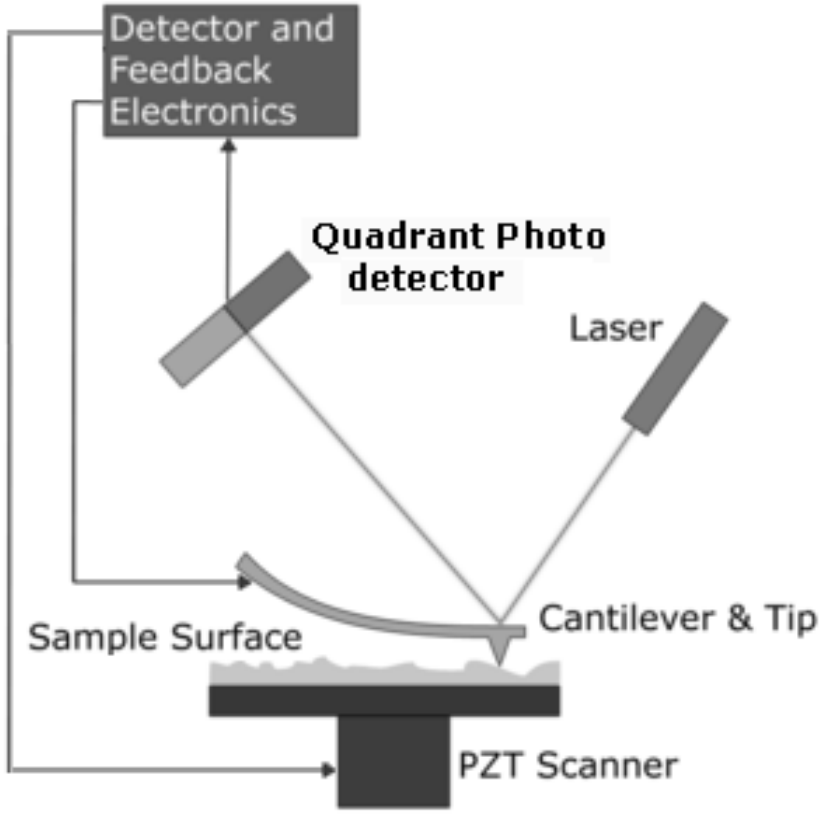

Figure 10: Schematic diagram of Atomic Force Microscope (AFM)

3.4 Optical Absorption

The equilibrium situation in semiconductor can be disturbed by generation of carriers due to optical photon absorption. Optical photon incident on any material may either be, reflected, transmitted or absorbed. The phenomena of radiation absorption in a material is all together considered to be due to 1) inner shell electrons, 2) valence band electrons, 3) free carriers including electrons and 4) electrons bound to localized impurity centers or defects of some type. In the study of fundamental properties of the semiconductors, the absorption by the second type of electrons is of great importance. In an ideal semiconductor, at absolute zero temperature the valence band would be completely full of electrons, so that electron could not be excited to higher energy state from the valence band. Absorption of quanta of sufficient energy tends to transfer of electrons from valence band to conduction band. The optical absorption spectra of semiconductors generally exhibits a sharp rise at a certain value of the incident photon energy which can be attributed to the excitation of electrons from the valence band to conduction band (may also involve acceptor or donor impurity levels, traps, excitons etc.) The conservation of energy and momentum must be satisfied in optical absorption process.

Basically there are two types of optical transitions that can occur at the fundamental edge of the crystalline semiconductor, direct and indirect. Both involve the interaction of an electromagnetic wave with an electron in the valence band, which is rose across the fundamental gap to the conduction band. However, indirect transition involves simultaneous interaction with lattice vibration. Thus the wave vector of the electron can change in the optical transition. The momentum change being taken or given up by phonon. Direct interband optical transition involves a vertical transition of electrons from the valence band to the conduction band such that there is no change in the momentum of the electrons and energy is conserved. The forms of the absorption coefficient 'α' as a function of photon energy *hv* depend on energy of NI for the bands containing the initial and final states. For simple parabolic bands and for direct transitions [31].

$$A = A\,(hv - Eg)^{n}/hv$$

Where A is a constant depending upon the transition probability for direct transition, n = ½ or 3/2 depending on whether the transition is allowed or forbidden in the quantum mechanical sense. Eg is the optical gap.

Let's visualize a situation given in Figure 18 (b) where interband transition takes place between different k-states. Since these must satisfy the momentum conservation laws, the only way such transition can take place is through the emission or absorption of a phonon with wave vector q i.e.

$$k' \pm q = k + K$$

Also for indirect transitions [37]

$$A = A\,(h\nu - Eg)^{n} / h\nu$$

For allowed transition n = 2 and for forbidden transitions n = 3. The band gap energy 'Eg' is determined by extrapolating the linear portion of the plot of $(\alpha h\nu)^{n}$ against hν to the energy axis at α = 0.

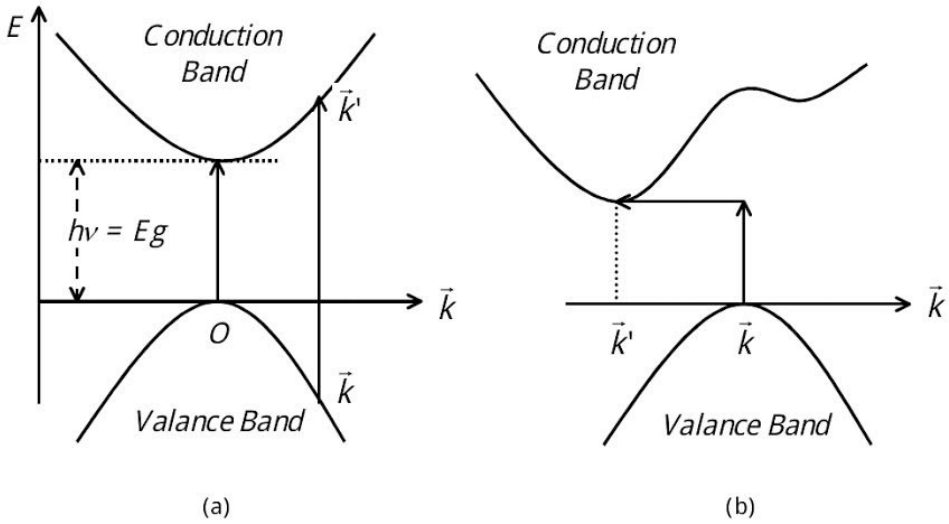

Figure 11: "Direct interband optical transitions" for a) direct band and b) indirect band semiconductors. The transitions are represented by vertical arrow.

3.5 Scanning electron microscope imaging

Scanning electron microscopy (SEM) is a widelyused surface analytical technique. SEM, accompanied by X-ray analysis, is considered a relatively rapid, inexpensive and basically non-destructive approach to surface analysis. High resolution images of surface topography, with excellent depth of field are produced using a highly-focused, scanning (primary) electron beam. The primary electrons enter a surface with high energy and generate many low energy secondary electrons. The intensity of these secondary electrons is largely governed by the surfacetopography of the sample. An image of the sample surface can thus be constructed by measuring secondary electron intensity as a function of the position of the scanning primary electron beam. High spatial resolution is possible because the primary electron beam can be focused to a very small spot (diameter < 10 nm). High sensitivity to topographic features on the outermost surface (< 5 nm) is achieved when using a primary electron beam with an energy of < 1 keV. In addition to low energy secondary electrons, backscattered electrons and X-rays are also generated by primary electron bombardment.

We used mainly the Raith 150 in our department, which has both SEM and EBL capabilities. Samples sputtered with ZnO were directly placed on a sample holder. Charging problems became more or less apparent, depending on the thickness of the (insulating) ZnO coating or whether the substrate was insulating. Toalleviate charging, a conductive layer was sometimes deposited over the sample, such as 10 nm of AuPd, or 5 nm of Ag.

3.6 Photoluminescence spectra measurements

The photoluminescence measuring technique is used for measuring the distribution of defects in a crystal.

Photoluminescence is the opticalemission obtained by photon excitation (usually a laser) and is commonly observed with semiconductor materials. This type of analysis allows non-destructive characterisation of the electronic structure of the band gap in semiconductor materials and can provide an indication of the nature of

structural and compositional defects within the material, such as the presence of unintentional dopants and surface related defects.

In this system, as shown in Figure 12, a helium-cadmium (HeCd) laser with an output power of 25 mW and a wavelength of 325 nm (UV light) acts as the excitation source. The light is focused onto the sample which is located in a cold finger liquid helium cryostat. For our measurements, the samples were cooled down to 4 K. The emitted photoluminescence (PL) is collected by a collimating lens before being focused into a spex1700 spectrometer for dispersion. A photomultiplier tube is used to measure the intensity of the PL over the range of wavelengths.

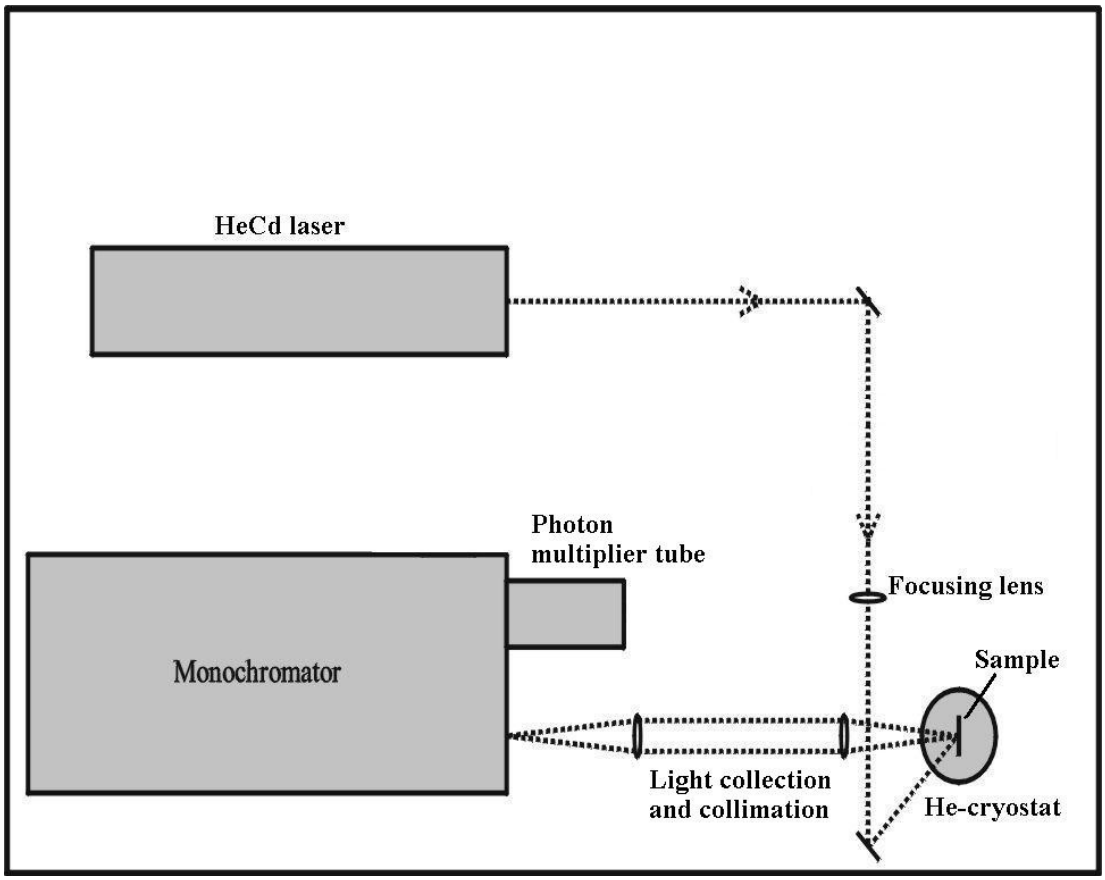

Figure 12: Schematic setup of PL measuring system.

Electrons in the sample are excited from the valence band to the conduction band, provided the photon energy from the laser is greater than the band gap of the material. In direct band gap semiconductors, such as zinc oxide, the electrons in the conduction band rapidly relax by emitting photons, corresponding to the band gap of the semiconductor. The electrons might also recombine with defects and perturbations within the lattice structure of the material, such as valence band holes.

These additional energy states may be investigated by examining the energy of the emitted photons.

CHAPTER 4

EXPERIMENTAL PRECEDURE

4.1 Substrates Preparetion

Amorphous glass slides with a thinkness of 3mm and size 15x15mm^2 were used as our subtrates during the experiment. The glass subtrates undergo a standard cleaning procedure to avoid dirt comtamination, which can effect the deposition rate directly.

- Detergent bath
- Stirred in Acetone for 10-15min
- Stirred in Ethanol for 10-15min
- Drying

4.2 Film deposition: Sputtering

ZnO thin films were deposited using NSC-3000 sputter coater (figure 12) also known as RF and DC magnetron sputtering machine. 99.99% zinc target of 50.8mm diameter and 3.18mm thinkness was used, figure 4.1 shows before and after used of the target, we experience there were small hole on the surface of the target. The zinc target and substrate were placed into the chamber seperated by 6cm above each other, the target was attached to the cathode and 4 glass subtrates were put on the lower part of the chamber (anode). The chamber was initially evacuated to 10^{-5} to 10^{-6} torr, because of the system pumped with a turbomolecular pump its only took 15-20min to obtained that very high vacuum.

Figure 13: Veiw of NSC-3000 Sputter Coater.

Then argon and oxygen gases were released into the chamber by flow rate of 20sccm for both, suddenly the pressure increased to 10^{-3} torr where the plasma came into visual contact. The process took 30min depositing the ZnO on our glass subtrates under high DC power of 200W.

At first we deposited the film without heating the substrates (i.e at room temperture) thereafter, we carried out exact several deposition by heating the subtrates to 100 ^{0}C, 200 ^{0}C, 300 ^{0}C and 400 ^{0}C.

Table 3: ZnO thin film deposition variables

DC Power (W)	Pressure (Torr)	Temperature (^{0}C)	Duration (Minute)
200	2.2×10^{-3}	RT	30
200	5×10^{-3}	100	30
200	5.4×10^{-3}	200	30
200	5.5×10^{-3}	300	30
200	4.8×10^{-3}	400	30

4.3 X-Ray Diffraction

The deposited ZnO crystalline phases were examined with a Rigaku x-ray diffractometer. The sample was placed in middle of the x-ray source and the detector. Cu-Kα radiation with a wavelength of 1.5406Å was used for diffraction, in the range of $2\theta = 30–70^0$ at a scan speed of 3^0/min and a step increment of 0.02^0 at room temperature. The x-ray voltage and current were held at 38KV and 28mA, respectively.

(a)

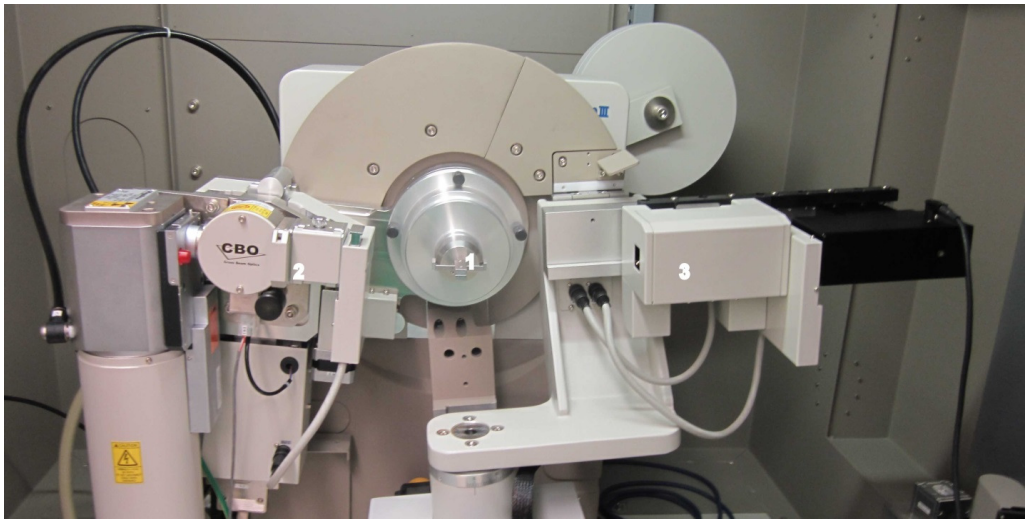

(b)

① Sample holder

② X-ray source

③ Detector

Figure 14: (a) Rigaku X-ray diffractometer. (b) Inside chamber of the XRD

From X-ray diffraction pattern we can obtain the following information:-

- To judge formation of a particular material system.
- Unit cell structure, lattice parameters, and miller indices.
- Types of phases present in the material
- Estimation of crystalline/amorphous content in the sample.
- Evaluation of the average crystalline size from the width of the peak in a particular phase pattern. Large crystal size gives rise to sharp peaks, while the peak width increases with decreasing crystal size.
- An analysis of structural distortion arising as a result of variation in *d*-spacing caused by the strain, thermal distortion.

Determination of crystal size:

The X-ray diffraction analysis has been the most popular method for the estimation of crystallite size in nanomaterials and therefore, has been extensively used in the present work. The evaluation of crystallite sizes in the nanometer range warrants careful analytical skills. The broadening of the Bragg peaks is ascribed to the development of the crystallite refinement and internal stain. To size broadening and stain broadening, the full width at half maximum (FWHM) of the Bragg peaks as a function of the diffraction angle is analyzed. Crystallite size of the deposits is calculated by the X-ray diffraction (XRD) peak broadening. The diffraction patterns are obtained using Cu-K_α radiation at a scan rate of 2^0/min. The full width half maxima (FWHM) of the diffraction peaks were estimated by pseudo-Voigt curve fitting. After subtracting the instrumental line broadening, which was estimated using quartz and silicon standards, the grain size can be estimated the Scherrer equation;

$$D = \frac{0.9\lambda}{\beta \cos\theta}$$

Where λ is the wave length of X-ray, β is the FWHM in radian, and θ is the peak angle

4.4 Atomic Force Microscopy (AFM)

Figure 15: Veiw of Nanomagnetics Atomic Force Microscope

The Nanomagnetics Atomic Force Microscope (AFM) system uses a laser beam to measure forces between micro-fabricated cantilevers and sample. A single piezo tube is used for scanning the sample in XYZ directions under computer control through the AFM Control Electronics and Software.

A red diode laser beam is focused at the back of the cantilever and the reflected beam hits a quadrant photodiode to measure the cantilever deflections as shown in Figure 23 the forces between tip and the sample deflect the cantilever and this change the position of laser beam on photo-detector. The use of quadrant photo-detector enables to measure formal as well as lateral forces action on the cantilever beam. The resultant photocurrents at the detector quadrants are amplified with a sensitive preamplifier and processed to give Normal Force (FNORMAL), Lateral Force (FLATERAL) and Total Force (FTOTAL) from the cantilever. The normal force is kept constant by adjusting the sample-tip separation using a piezo-ceramic

element (PZT) driven by a feedback circuit and high voltage amplifiers. As the sample is scanned in X and Y directions using the AFM Control Electronics, the feedback circuit moves the sample up and down keeping the force constant. Then the Z (x, y) position of the specimen, measured from the piezo voltage gives the topography of the surface.

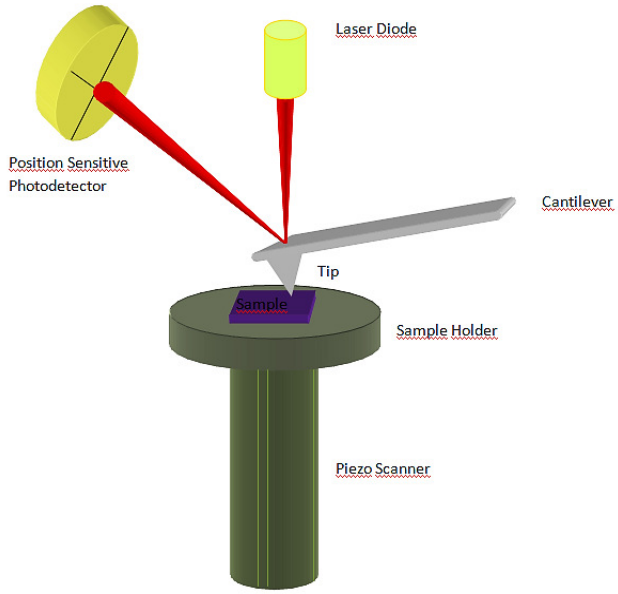

Figure 16: Principles of Atomic Force Microscopy.

4.5 UV-Visible Spectrophotometers

Figure 17: Veiw of Jasko V-530 Spectroscopy

A spectrophotometer is an instrument that measures the amount of optical absorption in a material, as a function of wavelength. In our case, the uv-vis spectroscopy wavelength range between 300-800nm. There are four components of a spectrophotometer; a light source, a monochromator, a sample chamber and a detector. We examined our samples using Jasko V-530 UV-Vis Spectrophotometer, our sample and a reference were put inside the chamber and we observe the absorption, transmission and reflectance of the light coming from the source after passing through the sample as shown schematically below.

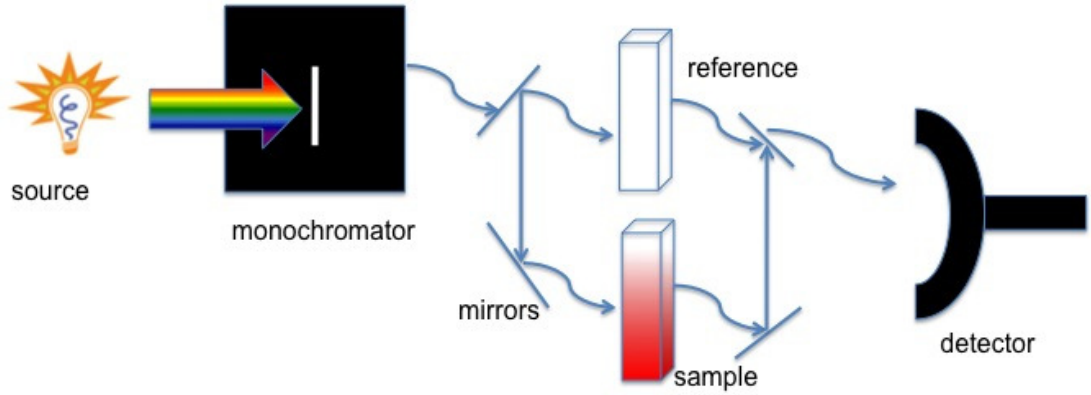

Figure 18: Schematic of UV-Vis spectroscopy.

And When light passes through or is reflected from the sample, the amount of light absorbed is the difference between the incident radiation (I_o) and the transmitted radiation (I). The amount of light absorbed is expressed as either transmittance or absorbance. Transmittance usually is given in terms of a fraction of 1 or as a percentage and is defined as

$$\alpha = \frac{2.303A}{t} \qquad \text{and} \qquad I = I_o e^{-\alpha t}$$

$$T = I/I_o \quad \text{or} \quad \%T = I/I_o \times 100$$

Where **α** is the absorption coefficient and **t** is the thickness of the sample (i.e the ZnO thin film).

And Absorbance is a dimentionless quantity defined as

$$A = -log_{10}T$$

CHAPTER 5

RESULT AND DISCUSSION

5.1 Introduction

In this chapter the results of the experimental work on the deposition and characterization of the sputtered ZnO thin film are presented. The results of the surface topography using Atomic Force Microscopy (AFM), crystallography of all the samples using X-Ray Diffractometer (XRD), optical absorption and transmission using Ultraviolet-Visible spectrophotometer.

5.2 Surface Topology

The surface topography and the roughness of our sputtered ZnO films based on the heated subtrates during deposition, were studied using Atomic Force Microscopy (AFM). According to what we observed from the images, the films smothness changes as the temperature increases during the deposition, indicating better smothness in the films. However, it can be also be observed that changing the substrate temperature has some effect on the surface roughness of the ZnO thin film. The images are shown in figure 1.

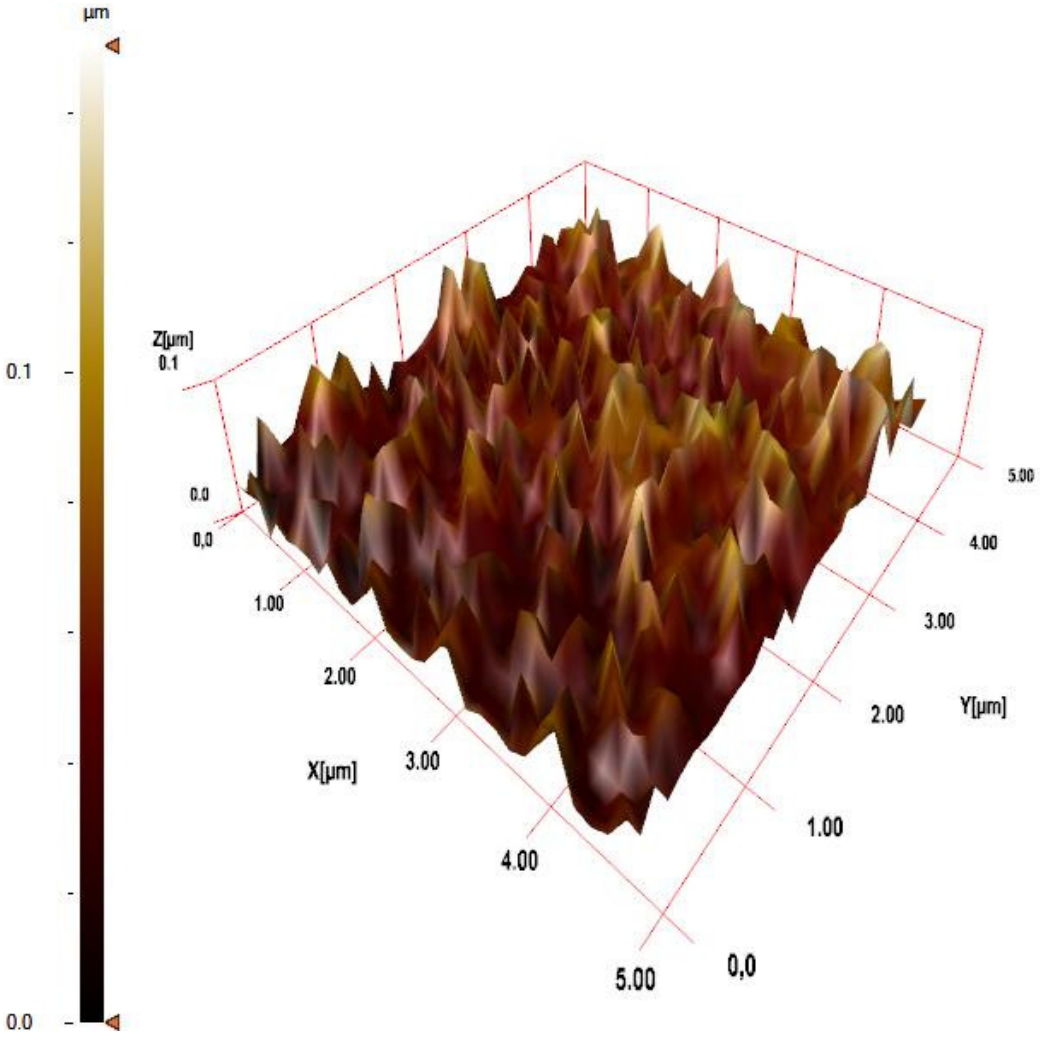

(*a*)

Figure 19: AFM images of ZnO thin films (a) at room temperature deposition, (b) at 100°C, (c) at 200°C, (d) at 300°, and (e) at 400°C.

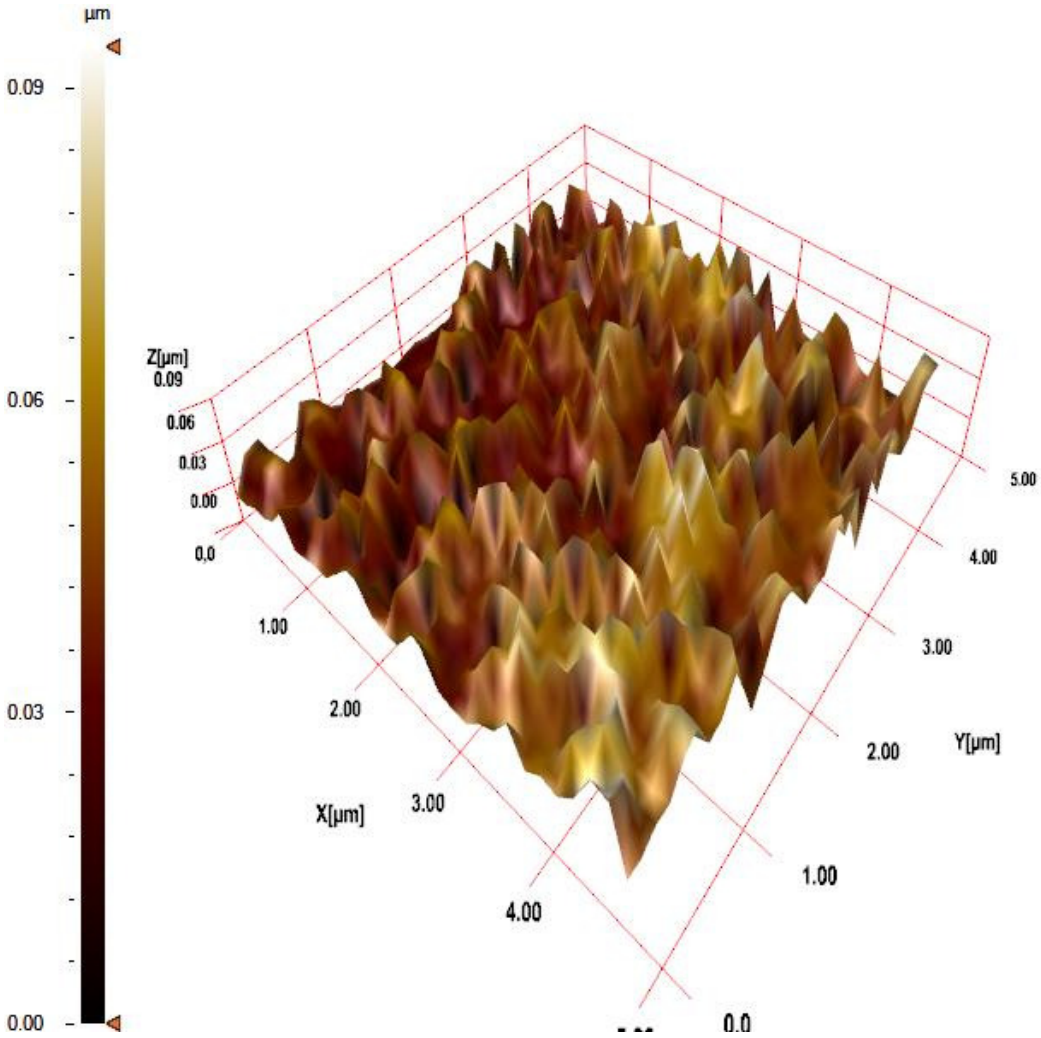

(b)

Figure 19 (continue): AFM images of ZnO thin films (a) at room temperature deposition, (b) at 100°C, (c) at 200°C, (d) at 300°, and (e) at 400°C.

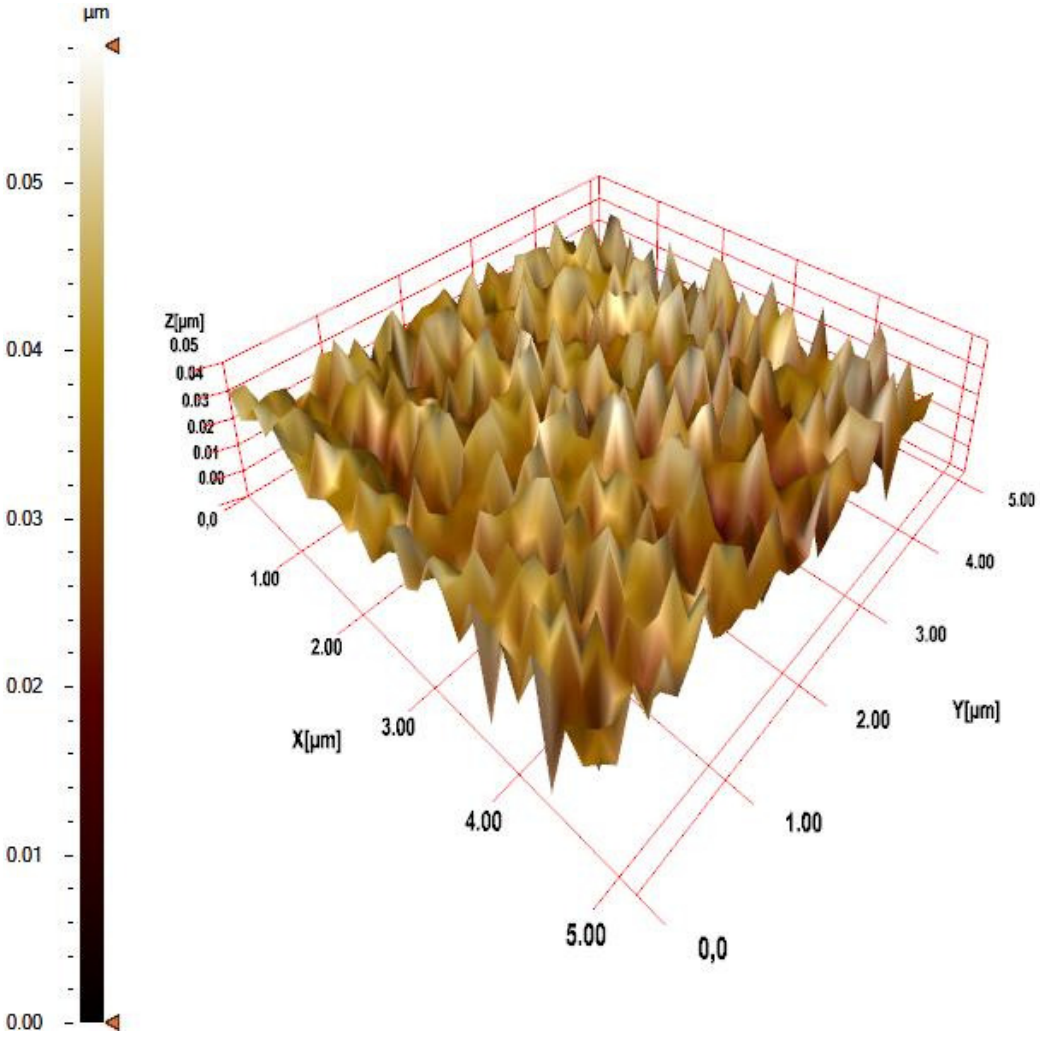

(c)

Figure 19 (continue): AFM images of ZnO thin films (a) at room temperature deposition, (b) at 100°C, (c) at 200°C, (d) at 300°, and (e) at 400°C.

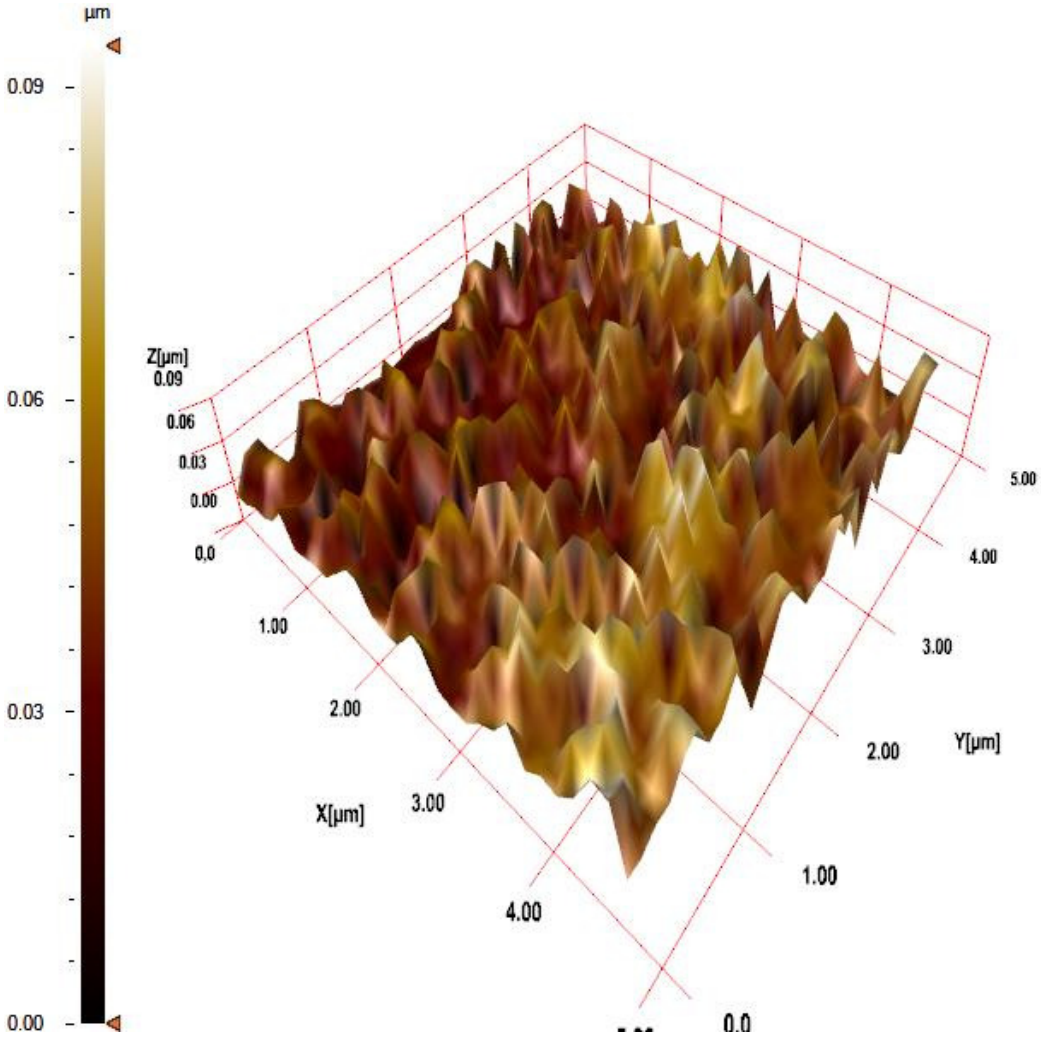

(d)

Figure 19 (continue): AFM images of ZnO thin films (a) at room temperature deposition, (b) at 100°C, (c) at 200°C, (d) at 300°, and (e) at 400°C.

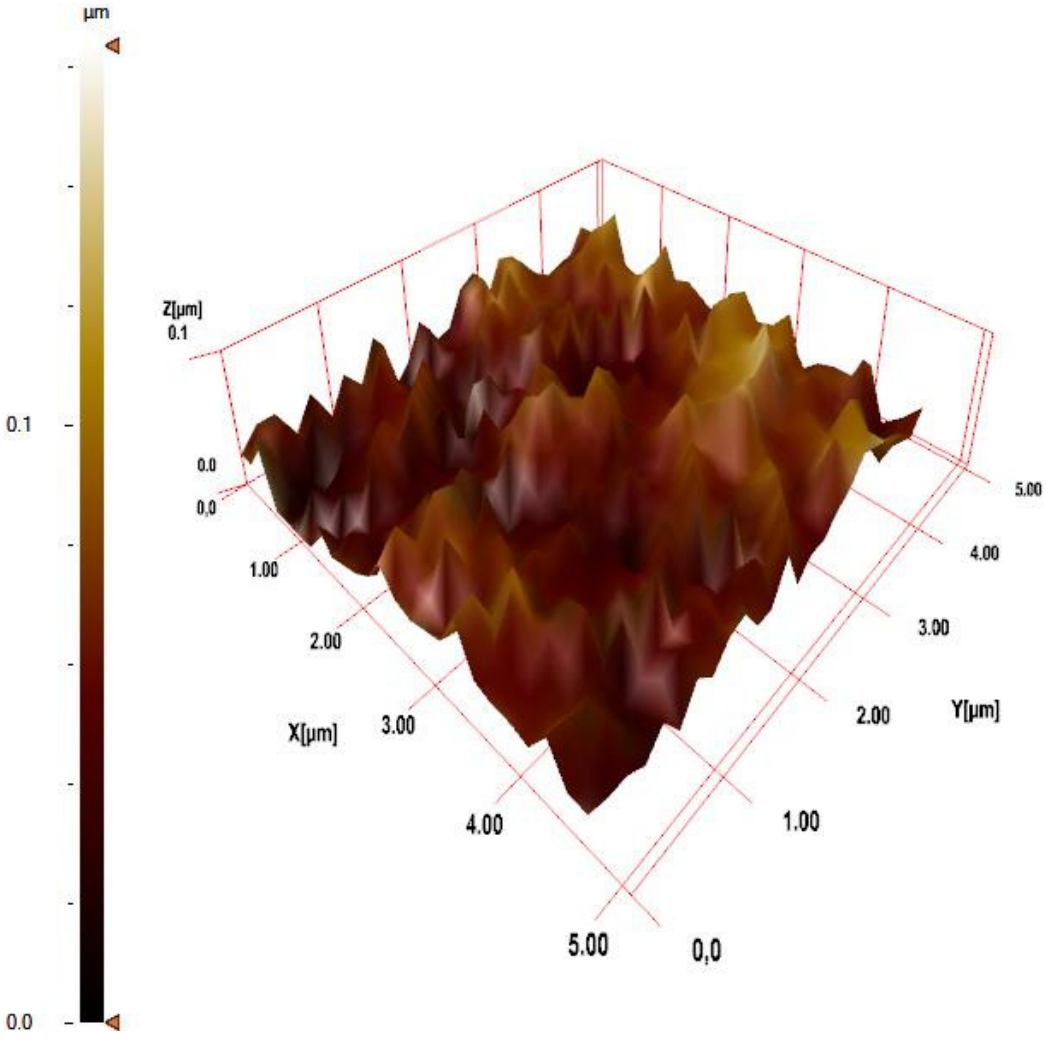

(e)

Figure 19: AFM images of ZnO thin films (a) at room temperature deposition, (b) at 100°C, (c) at 200°C, (d) at 300°, and (e) at 400°C.

5.3 Structural Characterization

The X-Ray diffraction spectra of our pure ZnO films are presented in figure 2. The films were produced based on the subtrate temperature (where the remaining variables held constant for all the films) from room temperature to 100 °C, 200 °C, 300 °C, and 400 °C. The diffraction angle 2θ was scanned in the range of 30°-70°

The intensity in arbitrary units is plotted against 2θ. It is seen from the figure the peaks appear mostly at ~34.2° which correspond to the lattice plain (002)-preffered orientation, which suggest that the film is aliged with *c-axis* oriented perpendicular to the substrate surface. The (002) plane happened to be strongest detection (*hkl*) peak. However, as the temperature of substrate reached 400 °C some peaks of much lower intensity were detected at 31.85°, 36.35°, 47.60°, 56.55°, and 62.29° corresponding to the following lattice plane (100), (101), (102), (110) and (103) respectively.

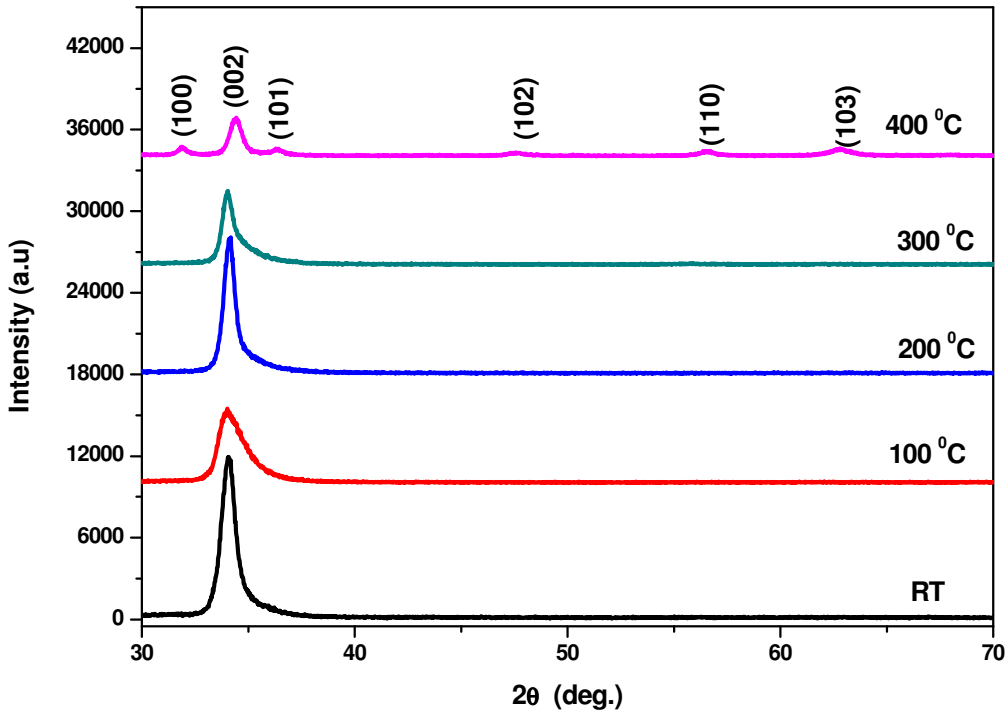

Figure 20: X-Ray diffraction pattern of ZnO for various deposition temperatures.

It is seen that the intensity as well as the Full-width-half-maximum (FWHM) of (002) peak is dependent on the deposition temperature and the film remain highly oriented with *c-axis* normal to the substrate. The position of (002) peak is shifted to a higher 2θ values from initial 34.05° (RT) to 34.42°. This could be due to the release of intrinsic strain through heating the substrate during the deposition.

As ZnO crystallizes in the Wurtzite structure in which the oxygen atoms are arranged in a hexagonal closed-packed type (*hcp*) with zinc atoms occupying half the

tetrahedral sites. Zn and O atoms are tetrahedrally coordinated to each other and have, therefore, an equivalent position. The zinc structure is open with all the octahedral and half the tetrahedral sites empty. The lattice constants a and c of Wurtzite structure ZnO were calculated, according to Bragg's law

$$2d \sin\theta = \lambda n,$$

Where n is the order of diffraction (usually n= 1), λ is the X-ray wavelength and d is the spacing between planes of given Miller indices h, k and l. In the ZnO hexagonal structure, the plane spacing is related to the lattice constants a, c and the Miller indices by the following relation.

$$\frac{1}{d^2_{(hkl)}} = \frac{4}{3}\left(\frac{h^2 + hk + k^2}{a^2}\right) + \frac{l^2}{c^2}$$

With the first order approximation, $n = 1$

$$\sin^2\theta = \frac{\lambda^2}{4a}\left[\frac{4}{3}(h^2 + k^2 + hk) + \left(\frac{a}{c}\right)^2 l^2\right]$$

$$a = \frac{\lambda}{2\sin\theta}\sqrt{\frac{4}{3}\left(h^2 + hk + \frac{l^2}{\left(\frac{c}{a}\right)^2}\right)}$$

$$c = \frac{\lambda}{2\sin\theta}\sqrt{\frac{4}{3\left(\frac{a}{c}\right)^2}(h^2 + hk + l^2)}$$

Table 4: Grain size, FWHM, lattice constant and plane distance of ZnO thin film at different deposition substrate temperature.

Substrate tempeture during deposition		RT	100 ^{0}C	200 ^{0}C	300 ^{0}C	400 ^{0}C
FWHM (002) peak		0.89555	1.55903	0.7379	0.95103	0.7258
Peak angle (deg.)		34.04877	34.23482	34.12497	34.112	34.41852
Grain size (nm)		16.94	9.737	20.57	15.96	20.93
Lattice constants	*a*(Å) (002)	3.18	3.16	3.17	3.17	3.15
	c(Å) (002)	5.26	5.23	5.25	5.25	5.21

5.4 Optical Properties

The optical transmittance of the film was measured using UV-Vis spectrophotometer in range of 350 to 800 nm. The transparency properties of all the films are more than 80% at visible light region. Moreover, it is observed that the transmittance has a tendency to decrease with the increase in substrate temperature. The reduction in the transmittance percentage is due to the increment of the temperature which slightly enlarges the particle size, as shown in AFM images. One of the vital parameter for the application of ZnO thin film is to have higher optical transmittance.

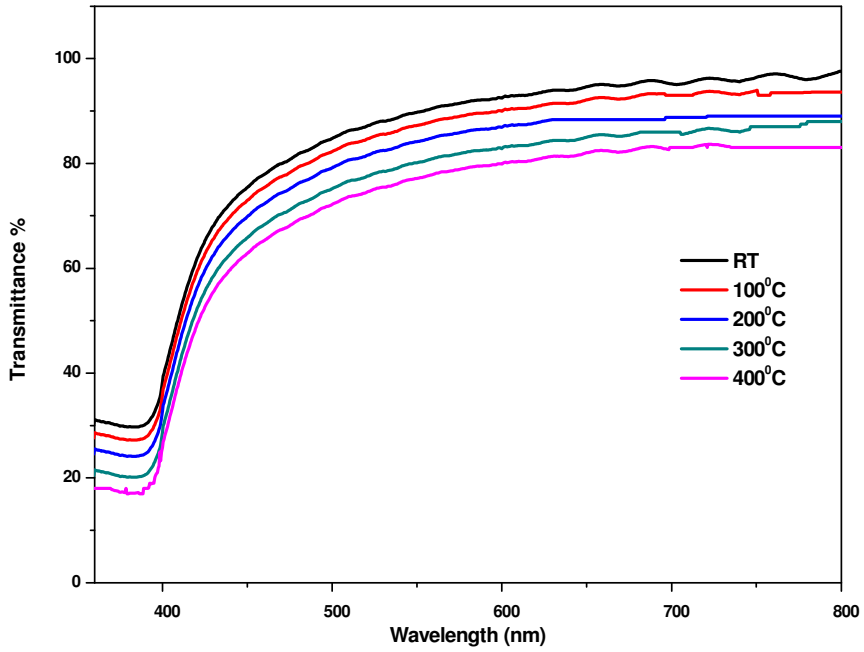

Figure 21: Optical transmittance spectra of ZnO thin film based on the various deposition temperatures

Also the absorption coefficient was calculated using the transmittance data, which has been presented previously. Lambert's law has been applied to obtain the value of absorption coefficient at a respective wavelength.

$$\alpha = \frac{1}{t}\ln\left(\frac{1}{T}\right)$$

Where, t is the film thickness and T is the transmittance spectra of the films. The result indicates that all films exhibit high absorption in the ultra violet (UV) region and low absorption in the visible light region. The coefficients in the UV region significantly decreased with the increase in deposition substrate temperature. The results suggested a better optical absorption at low temperature of the substrates which can provide useful information especially in the optoelectronic devices and device fabrication.

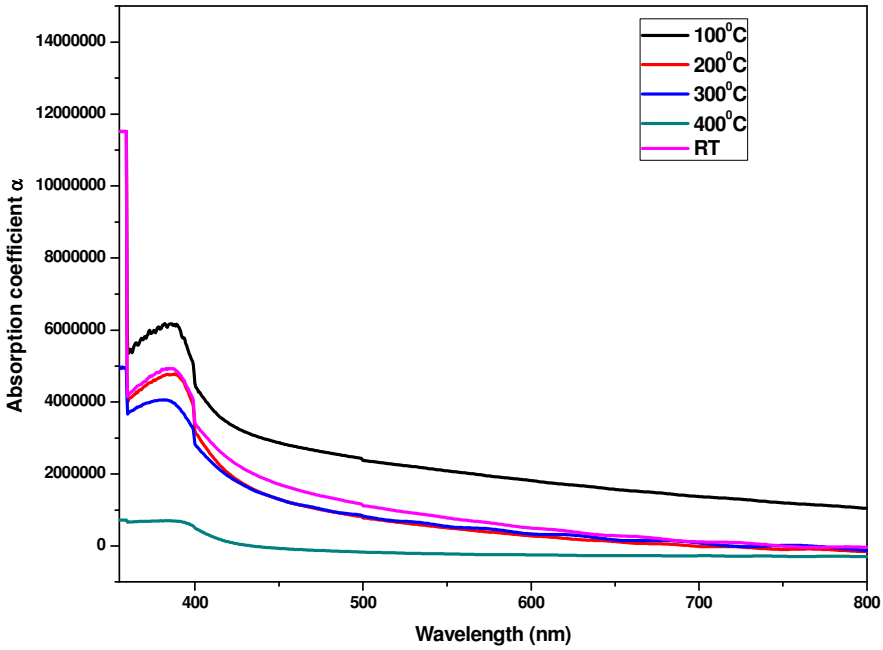

Figure 22: Absorption coefficient of ZnO thin at various deposition substrates temperature

Figure 22 represent energy band gap of the ZnO films, which show a presence of a single slope to all substrate temperature dependent ZnO films. The plot shows that the films have direct and allowed transition and it is well known that ZnO is a direct band-gap semiconductor and the energy gap can thus be estimated by assuming direct transition between conduction band and valence bands.

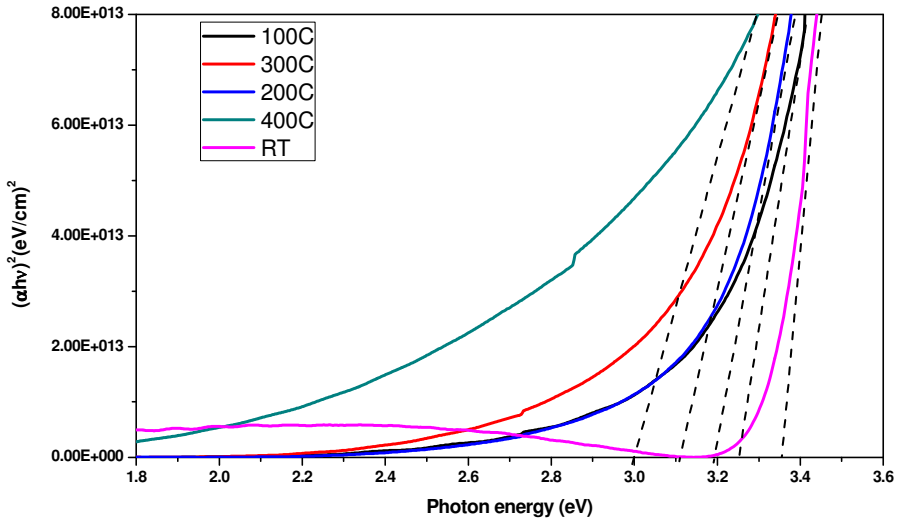

Figure 23: Optical energy band gap of ZnO thin film at different deposition substrate temperation.

The optical band gap shows an increase when the substrate temperature two decreases as shown in table 1. This implies that when substrate temperature increases energy gap between conduction and valence band narrowed which makes carrier electron to jump easier from valence to conduction band which means, as the substrate temperature increases our ZnO films become more unstable.

Table 5: Optical energy band gaps at a specific deposition substrate temperatures.

Substrate temperature (°C)	Optical energy band gap (eV)
RT	3.353
100	3.257
200	3.209
300	3.137
400	3.003

Figure 5 shows the measured optical band gap energies versus substrate temperatures. For room temperature ZnO thin film, the optical band gap energy is 3.353eV which is slightly higher compared to other reports [1,2] with an increment in substrate temperature the band gap decreases to 3.257, 3.209, 3.137, and 3.003 eV for 100, 200, 300, and 400 °C respectively. A decrement of about 0.34eV in the

optical band gap was obtained. This evidently shows that the band gap of ZnO thin film can altered.

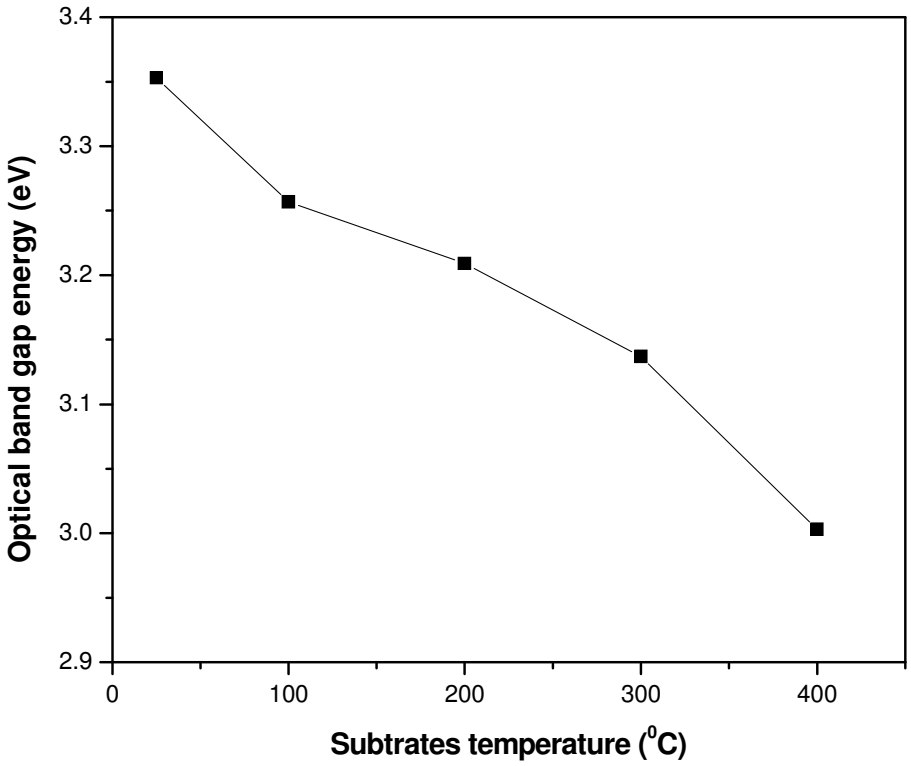

Figure 24: Variation of energy band gap against substrates temperature.

The best optical performance of all samples was observed at RT deposition temperature due to its higher transmittance and the photoactive performance was obtained at the highest deposition temperature i.e. 400 °C due to the excess thermal energy generated by heating the substrates during the film deposition.

CHAPTER 6

CONCLUSION

ZnO thin films were grown on soda lime glass substrate by reactive sputtering method at different deposition temperature, from RT to 400 °C. According to XRD results, ZnO film a (002)-preferred orientation was observed, which suggests that the film is aligned with the *c-axis* oriented perpendicularly to the glass substrate surface. The effect of the substrate temperature during deposition on the crystallinity, optical properties, and surface topology of sputtered ZnO were analyzed. According to XRD analysis, decrease in (002) diffraction intensity of XRD pattern was observed as the substrate temperature increases. Also, the position of the (002) peaks shifted to a higher 2θ values, which could be due to the release of intrinsic strain through heating the substrate. The reasonably changes in FWHM values in XRD pattern demonstrate higher crystal quality of the ZnO thin film at some specific temperature of the substrates. The lattice constant *a* and *c* were determined and observed to be decreasing as the substrate temperature increase. Slightly smaller values for both *a* and *c* parameter compared to RT samples.

AFM studies help us to analyze the surface topology of ZnO thin films, the films were formed from nanocrystals, with preferential *c-axis* perpendicular to the substrate surface, AFM demonstrate that the film roughness changes as the temperature increases, indicating better smoothness in the films. The rms values decreases.

According to optical characterization, all the films exhibit a high transparency in the visible region. From the transmission spectra curves corresponding to the increase in the deposition temperature of the samples, one can conclude that as the temperature increases: a decrease of the optical transmittance intensity in the visible region was obtained as compared with RT samples. And also some slightly little changes of the energy bandgap of the ZnO thin films were observed, which decreases

as temperature increase compared with the RT samples. Finally, the properties of the sputtered ZnO thin film due to the increase in substrate temperature during deposition can technically affect the optoelectronic application such as LED, photodetector and laser diodes [36], but also suitable for solar cell application.

BIBLOGRAPHY

[1] Introduction to solid state physics by Charles Kittle 8th edition.

[2] Principles of semiconductor devices by B. Van Zeghbroeck.

[3] Consequences of the Maxwell–Boltzmann Distribution Chapter 9 by Dario Camuffo

[4] Sintering Reactions of Zinc Oxide, Journal of Applied Physics, 1959. By V.J Lee and Parravano G.

[5] Non-linear varistors using oxides of zinc, silicon and tin by Valeev, K.S., V.A. Knyazev, and N.O. Drozdov. Elektrichestvo, 1964.

[6] Recent advances in processing of ZnO. Journal of Vacuum Science & Technology B, by S.J Pearton, D.P. Norton, K. Ip, Y.W. Heo and T. Steiner.

[7] Ultraviolet detectors in thin sputtered ZnO films by, Henrik Fabricius, Torben Skettrup, and Paul Bisgaard.

[8] Investigation of lateral parameter variations of Al-doped zinc oxide films prepared on glass substrates by RF magnetron sputtering by Dengyuan Song, Per Widenborg, Winston Chin, Armin G. Aberle

[9] Variation of light emitting properties of ZnO thin films depending on post-annealing temperature by Hong Seong Kang, Jeong Seok Kang, Seong Sik Pang, Eun Sub Shim, Sang Yeol Lee.

[10] Fundamentals of zinc oxide as a semiconductor by Anderson Janotti and Chris G Van de Walle.

[11] Recent progress in processing and properties of ZnO by S.J. Pearton, D.P. Norton, K. Ip, Y.W. Heo, T. Steiner.

[12] Recent advance in biosensors by A.F. Collings and Frank Caruso. 1997.

[13] Sputtered zinc oxide coatings: structural study and application to the photo protection of the polycarbonate by A. Moustaghfir, E. Tomasella, A. Rivaton, B. Mailhot, M. Jacquet, J.L. Gardette, J. Cellier.

[14] W. L. Bond, Acta Crystallogr. 13, 814 (1960)

[15] A. B. M. A. Ashrafi, A. Ueta, A. Avramescu, H. Kumano, I. Suemune, Y.-W. Ok, and T.Y. Seong, Appl. Phys. Lett. 76, 550 (2000).

[16] W.J. Fan, J.B. Xia, P.A. Agus, S.T. Tan, S.F. Yu and X.W. Sun JOURNAL OF APPLIED PHYSICS 99, 013702 (2006).

[17] A.R. West, 'Solid State Chemistry' John willey & Sons, Singapore, (2003).

[18] K. L. Chopra,'Thin Film Phenomena', McGraw Hill, New York (1969)

[19] Y. Gao, H. Niu, C. Q. Chen, Chem. Phys. Lett., 367 (2003) (1-2) 141

[20] Singh, R., M. Kumar, and S. Chandra, Growth and characterization of high resistivity c-axis oriented ZnO films on different substrates by RF magnetron sputtering for MEMS Applications. Journal of Materials Science, 2007. 42(12): p. 4675-4683.

[21] Anderson, A.C. and D.E. Oates. RF magnetron sputtering of ZnO for SAW: effects of Magnetic field strength and configuration. 1982. San Diego, CA, USA: IEEE.

[22] Kappertz, O., et al., Reactive sputter deposition of zinc oxide: Employing resputtering effects to tailor film properties. Thin Solid Films, 2005. 484(1-2): p. 64-67.

[23] The dependence of structural and optical properties of PLD grown ZnO films on ablation parameters. Arun Aravinda, M.K. Jayaraja, Mukesh Kumarb, Ramesh Chandrab

[24] Pulsed Laser Deposition (PLD) - a Versatile Thin Film Technique Hans-Ulrich Krebs, Martin Weisheit, Jörg Faupel, Erik Süske, Thorsten Scharf, Christian Fuhse, Michael Störmer, Kai Sturm, Michael Seibt, Harald Kijewski, Dorit Nelke, Elena Panchenko, and Michael Buback

[25] Basics of Molecular Beam Epitaxy (MBE) by Fernando Rinaldi

[26] Growth and doping of gallium arsenide using molecular beam epitaxy (MBE): Thermodynamic and kinetic aspects R. Heckingbottom, G.J. Davies, K.A. Prior

[27] Hetero-epitaxial growth of ZnO thin films by atmospheric pressure CVD method.

Y. Kashiwaba, F. Katahira, K. Haga, T. Sekiguchi H. Watanabe.

[28] Thin Solid Films K. Haga, K. Katahira, H. Watanabe, (1999) 145.

[29] The Scattering of X-rays and Bragg's Law By G.E.M Jauncey.

[30] B.D. Cullity, Elements of X-rays 2nd edition Addiso Wesley, London, (1978).

[31] C. S. Barrett and T.B. Massalski, “Structure of metals”, McGraw-Hill, New York, (1966).

[32] Introduction to Atomic Force Microscopy Theory, Practice and Application. By Paul E.West

[33] F. Micheltti and P. Mark, J. Appl. Phys. Lett., 10 (1967) 136.

[34] E. Becquerel, Comt. Rend. H. A. 9 (1839) 561.

[35] B.D. Cullity, S. Rstock, Elements of X-ray Diffraction, Prentice Hall, New Jersey, 2001

[36] ZnO-Based Light-Emitting Diodes by J.C. Fan, S.L. Chang and Z. Xie